

ME 407: Computational Fluid Dynamics

Pavan Kapoor, Spencer Kirsch, Jude Pizzone, Allen Rakhamimov

Final Design Project

Instructor: Professor Scott Bondi

May 2025

Contents

Executive Summary	1
Design	1
Performance	2
Design	4
Design Assumptions and Concepts	4
Sketches of Design	5
Model	5
Engineering Drawings	9
Simulation	10
Meshing	10
Simulation	12
Model Fitting	23
Results	24
Verification	27
Thermodynamic Calculations	27
Vane & Blade Design Calculations	28
Efficiency Calculations	30
Conclusion	31

References	32
Appendix A: Maximum Altitude Simulation Results by Submodel	32
Appendix B: Sea Level Simulation Results by Submodel	45

List of Figures

1	CAD model of axial compressor design.	1
2	Front view of the CAD of the compressor.	6
3	Isometric view of the CAD of the compressor.	6
4	Sliced side view of compressor CAD	7
5	Sliced isometric view of compressor CAD	8
6	CAD drawing of axial compressor design.	9
7	Mesh of stage 2.	11
8	Element quality of the stage 2 mesh.	11
9	Minimum and maximum aspect ratios of the stage 2 mesh.	12
10	Pressure contour of stage 1 simulation at 40,000 ft above sea level.	13
11	Temperature contour of stage 1 simulation at 40,000 ft above sea level.	13
12	Velocity streamline plot of stage 1 simulation at 40,000 ft above sea level.	14
13	Velocity vector plot of stage 1 simulation at 40,000 ft above sea level.	15
14	Alternative view of velocity vector plot of stage 1 simulation at 40,000 ft above sea level.	16
15	Static pressure convergence plot of stage 1 simulation.	17
16	Temperature convergence plot of stage 1 simulation.	17
17	Mass flow rate convergence plot of stage 1 simulation.	18
18	Scaled residual plot of stage 1 simulation.	18
19	Pressure contour of stage 2 simulation at 40,000 ft above sea level.	19
20	Temperature contour of stage 2 simulation at 40,000 ft above sea level.	19

21	Pressure contour of stage 3 simulation at 40,000 ft above sea level.	20
22	Temperature contour of stage 3 simulation at 40,000 ft above sea level.	20
23	Pressure contour of stage 1 simulation at STP.	21
24	Temperature contour of stage 1 simulation at STP.	21
25	Pressure contour of stage 2 simulation at STP.	22
26	Temperature contour of stage 2 simulation STP.	22
27	Comparative simulation and hand calculated values for maximum operating altitude pressures and temperatures per stage	24
28	Hand Calculated efficiency calculation for Stage 1 at maximum altitude (top) and sea level (bottom).	25
29	Temperature convergence plot at stage 1.	33
30	Pressure convergence plot at stage 1.	34
31	Mass flow rate convergence plot at stage 1.	34
32	Scaled residual plot at stage 1.	35
33	Pressure convergence plot at stage 2.	35
34	Mass flow rate convergence plot at stage 2.	36
35	Scaled residual plot at stage 2.	37
36	Temperature convergence plot at stage 3.	38
37	Pressure convergence plot at stage 3.	39
38	Mass flow rate convergence plot at stage 3.	40
39	Scaled residual plot at stage 3.	41
40	Temperature convergence plot at stage 4.	42
41	Pressure convergence plot at stage 4.	43
42	Mass flow rate convergence plot at stage 4.	44
43	Scaled residual plot at stage 4.	45
44	Temperature convergence plot at stage 1 at ground.	46
45	Pressure convergence plot at stage 1 at ground.	47
46	Mass flow rate plot at stage 1 at ground.	47
47	Scaled residual plot at stage 1 at ground.	48

48	Temperature convergence plot at stage 2 at ground.	48
49	Pressure convergence plot at stage 2 at ground.	49
50	Mass flow rate plot at stage 2 at ground.	49
51	Scaled residual plot at stage 2 at ground.	50

List of Tables

1	Performance metrics for maximum operating altitude.	2
2	Performance metrics at sea level.	2
3	Design parameters.	3
4	Mesh statistics for first four compressor stages	10
5	Results for simulations at maximum operating altitude of 40,000 feet are compared to hand calculations. Quantities with blue infill are extrapolated based on an exponential model fitted with simulation data.	26
6	Results for simulations at sea level are compared to hand calculations. Quantities with blue infill are extrapolated based on an exponential model fitted with simulation data.	26
7	Standard conditions and properties of air at an altitude of 40,000 feet [3], [1], [2].	27
8	Tabulated inlet and outlet conditions after 17 stages based on ideal, isentropic compressor approximation.	28

Executive Summary

Our objective was to design a compressor stage for a jet engine. The compressor was required to be contained within a total outer diameter between 5 to 6 feet with an outlet to inlet pressure ratio of 20 to 1 at the maximum operating altitude, 40,000 feet. The maximum revolution rate was 50,000 rpm. Operating characteristics were requested at maximum operating altitude and sea level.

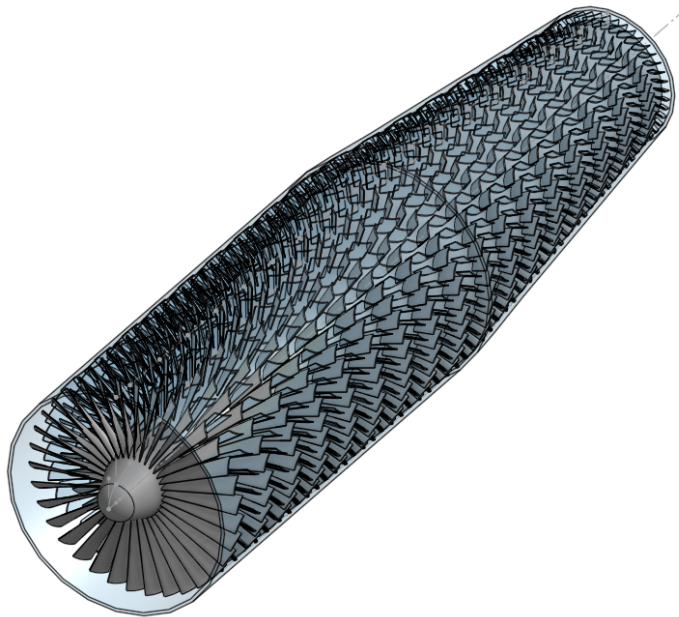


Figure 1: CAD model of axial compressor design.

Design

Our design pictured in Figure 1 is an axial compressor due to its scalability and prevalence in modern aeronautics. Each stage set was designed to have a compression ratio of 1.2:1, then the appropriate amount of stages were included to achieve the design ratio of 20:1. Computational Fluid Dynamics software ANSYS Fluent was used to simulate our design and verify design decisions based on analytical calculations and thermodynamic theory. A fully parametric seventeen stage axial compressor was designed in CAD to be able to easily edit parameters such as AOA of the rotor and stator blades at the hub and at the tip, annular area at each stage, chord length of each rotor and stator blade and the number blades in each stage. This allowed us to rapidly iterate through different designs and leverage our simulation results to optimize our axial compressor design.

Performance

The design achieves a simulated pressure ratio of 38:1 and hand calculated to be 22:1 at the maximum operating altitude of 40,000 feet, heating up the air by 1500°F in simulation or 500°F by hand calculation. At sea level, the simulated pressure ratio of 15:1 and hand calculated to be 22:1 at the maximum operating altitude of 40,000 feet, heating up the air by 1300°F in simulation or 800°F by hand calculation. Complete simulated performance metrics are enumerated in Tables 1, 2, 3.

Table 1: Performance metrics for maximum operating altitude.

40,000 Feet	Inlet	Outlet	Unit
Ambient Pressure	2.7	103	psi
Ambient Temperature	-69.7	1592	F

Table 2: Performance metrics at sea level.

Sea level	Inlet	Outlet	Unit
Ambient Pressure	14.7	223	psi
Ambient Temperature	59.0	1253	F

Table 3: Design parameters.

Parameter	Value	Unit
Rotational speed	2500	rpm
Outer Diameter	5.96	ft
Length	23.4	ft
Maximum blade length	25.8	in
Minimum blade length	3.2	in
Dry Mass	11000	lbm
Blade/Vane shape	NACA 9506	n/a
Power at 40k	1087	HP
Compression Ratio 40K	22	
Power at STP	4902	HP
Compression Ratio STP	22	

Design

Design Assumptions and Concepts

To achieve a total pressure ratio of at least 20:1, we designed for the pressure ratio through each rotor/stator set to be 1.2:1. We can then chain these together to achieve the desired complete pressure ratio. To meet our design pressure ratio of 1.2:1 per stage, we need to reduce the annular area after each stage. We start from momentum conservation in an ideal, isentropic compressor.

$$\rho_1 \vec{v}_1 A_1 = \rho_2 \vec{v}_2 A_2$$

The axial velocity does not meaningfully change across the compressor, therefore $v_1 = v_2 = v_{\text{inlet}}$. This leads to the following relationship for how annular area is restricted per stage. The derivation of density ratio can be found in the Section **Thermodynamic Calculations**, on page [28](#).

$$A_2 = A_1 \frac{\rho_1}{\rho_2} = A_1 \frac{\rho_1}{1.13922\rho_1} = 0.87779A_1$$

To maximize available airflow, we choose the diameter to the blade tips to be 5.8 feet throughout the whole compressor, denoted the “tip diameter,” d_o . We choose the starting rotor “hub diameter”, d_i to be 1.5 feet. The operating rotational rate is 2500 rpm. The hub diameter expands down the compressor to smoothly restrict the annular area. The area of an annular region defined between inner radius r_i and outer radius r_o is

$$A = \pi r_o^2 - \pi r_i^2 = \pi(r_o^2 - r_i^2)$$

We can express the annular area in terms of diameters $d_i = 2r_i$ and $d_o = 2r_o$ and solve for the required hub diameter for adequate restriction.

$$\begin{aligned} A &= \frac{\pi}{4}(d_o^2 - d_i^2) \\ A &= \frac{\pi}{4}d_o^2 - \frac{\pi}{4}d_i^2 \\ \frac{\pi}{4}d_i^2 &= \frac{\pi}{4}d_o^2 - A \\ d_i^2 &= d_o^2 - \frac{4}{\pi}A \\ \implies d_i &= \sqrt{d_o^2 - \frac{4}{\pi}A} \end{aligned}$$

Finally we can determine the blade length b for each stage.

$$b = r_o - r_i = \frac{d_o - d_i}{2}$$

Further computations are enumerated in the **Verification** section.

Sketches of Design

The compressor was modeled in OnShape by parameterizing stage width, stage hub and tip radii, chord length and spacing, rotor and stator blade angles, number of blades, blade angles, and major and minor annular areas. The overall length of the designed compressor was 281.101 inches, with an outer diameter of 71.60 inches at the inlet and 42.240 inches at the outlet. The total mass (assuming the material is aluminum) is 11000 pounds.

Model



Figure 2: Front view of the CAD of the compressor.

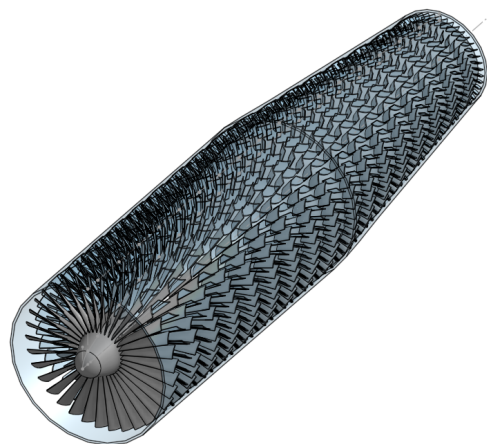


Figure 3: Isometric view of the CAD of the compressor.

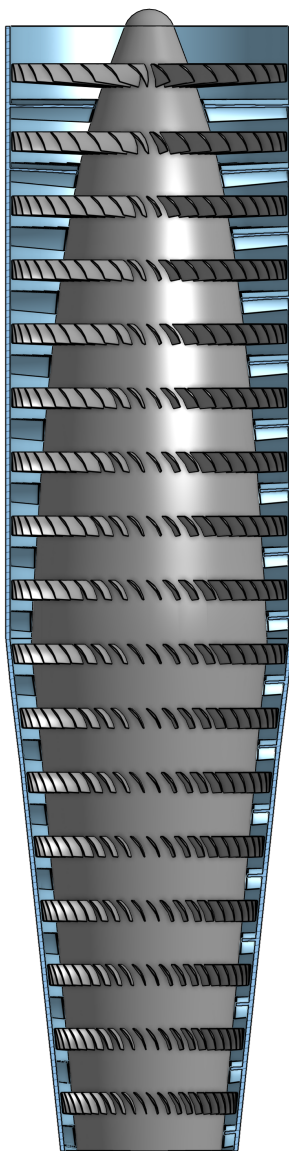


Figure 4: Sliced side view of compressor CAD

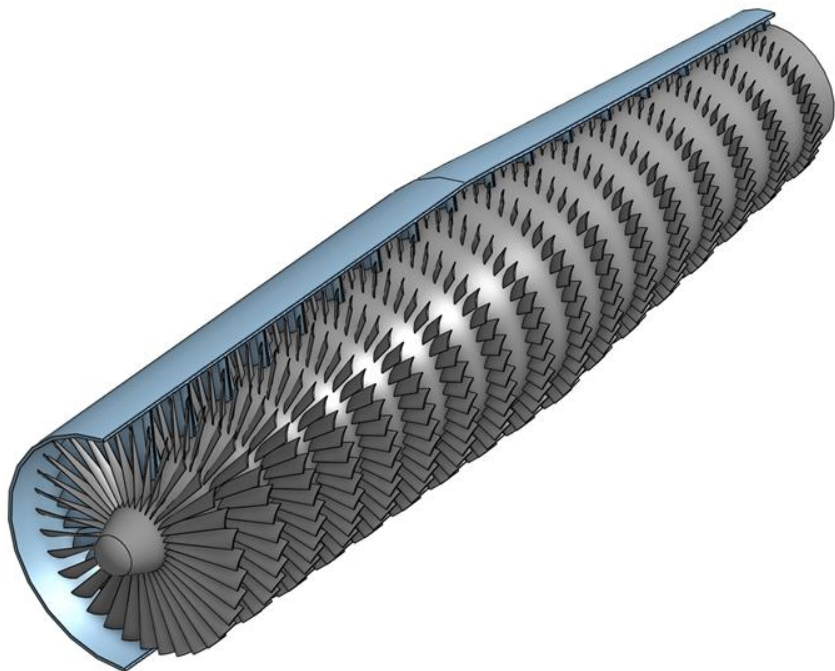


Figure 5: Sliced isometric view of compressor CAD

Engineering Drawings

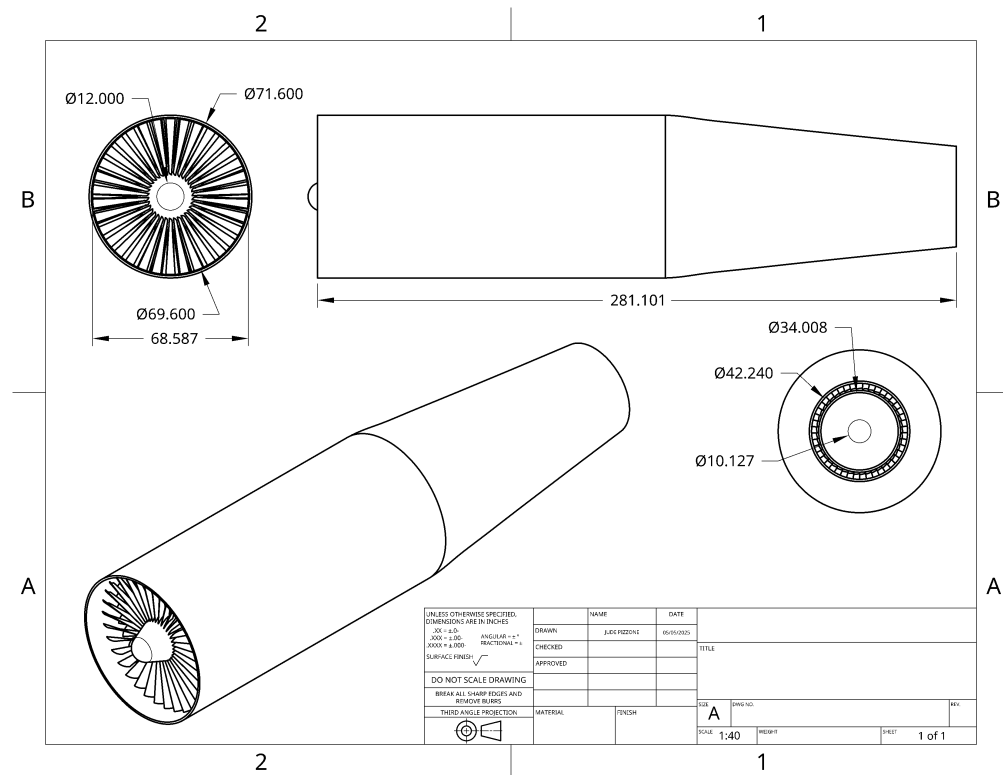


Figure 6: CAD drawing of axial compressor design.

Simulation

Each stage was meshed and simulated separately, in series, such that the mean outlet condition of a preceding stage serves as the inlet condition of the following stage. Four stages were simulated completely, then the data was fitted to an exponential model following thermodynamic theory on page 28. ANSYS Fluent was used for each simulation.

Meshing

Meshing was performed with ANSYS Meshing in Workbench. Each mesh had patch conforming method and a body sizing of 0.5 in. All meshes had an inflation on all face except inlets and outlets of 3 layers, 1.2 growth rate, and adaptive mesh sizing with a resolution of 7.

Table 4: Mesh statistics for first four compressor stages

Mesh	Max Aspect Ratio	Minimum Element Quality	Body sizing (in)
Rotor 1	9.89	0.15	.5
Stator 1	10.84	0.15	.5
Rotor 2	9.07	0.14	.5
Stator 2	9.53	0.17	.5
Rotor 3	9.22	0.17	.5
Stator 3	10.22	0.16	.5
Rotor 4	9.87	0.15	.5
Stator 4	10.86	0.15	.5

These mesh statistics were used to create our meshes for each stage.

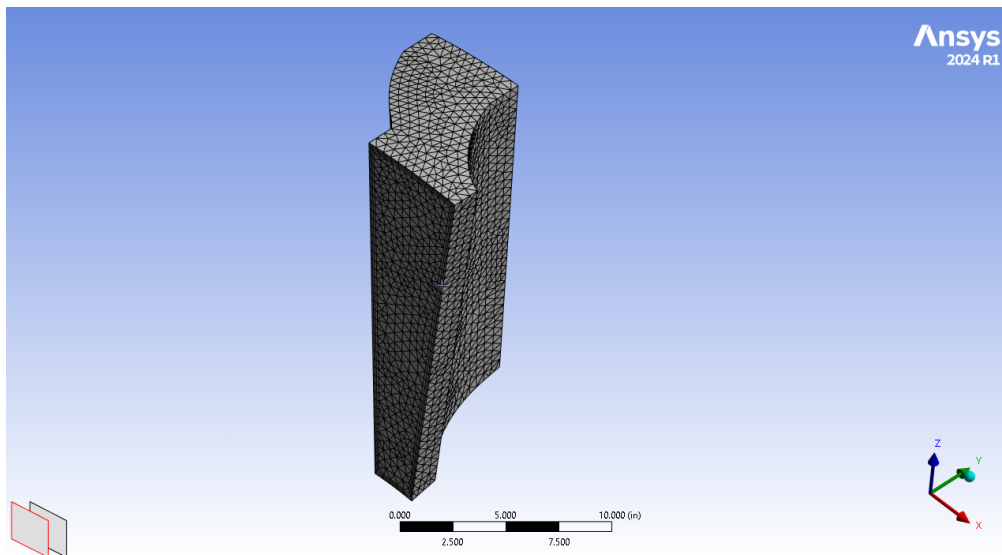


Figure 7: Mesh of stage 2.

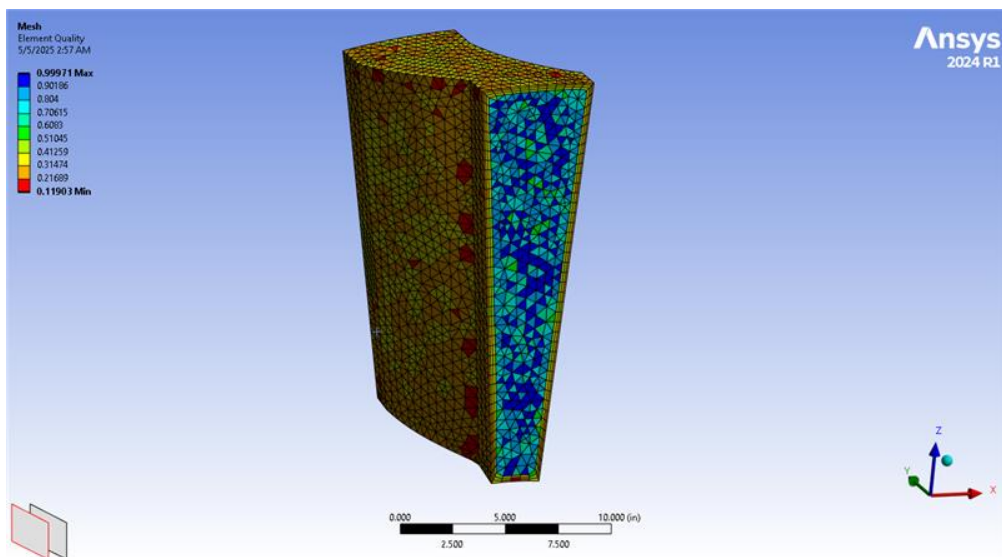


Figure 8: Element quality of the stage 2 mesh.

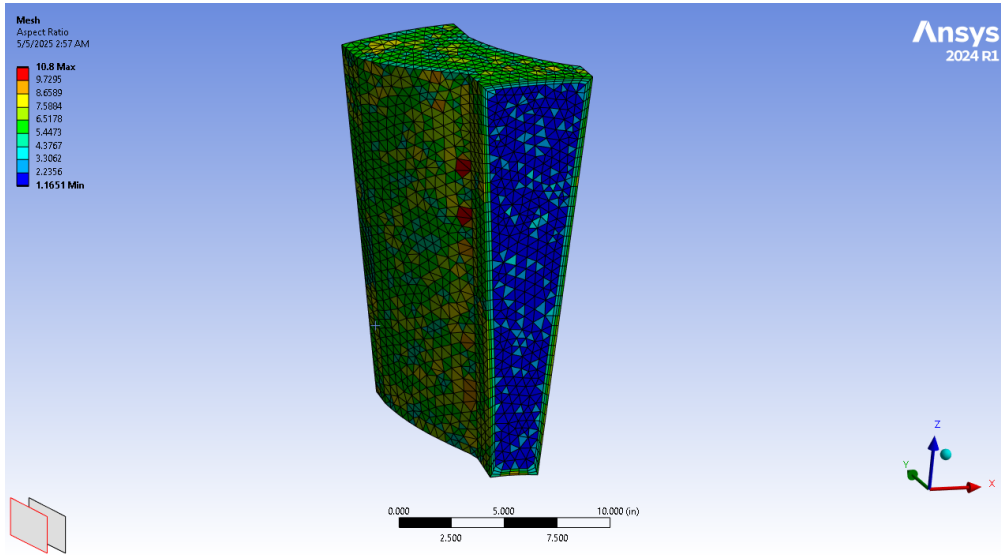


Figure 9: Minimum and maximum aspect ratios of the stage 2 mesh.

Simulation

The simulation settings were set to a pressure-based solver and transient time in double precision.

The operating pressure was set to 0 psi. The pressure inlet was set with the total gauge pressure at 2.73 psi, the initial gauge pressure at 1.86 psi and total temperature at -19.95 degrees Fahrenheit (which is the total temperature input, that is, $T_{\text{static}} + \frac{v^2}{2cp}$). For subsequent stages, the area average static and total pressure and temperatures of the outlet of the previous stages were used as the inlet boundary conditions. A mesh interface with periodic repeats was created between the rotor and the stator.

Rotational periodic boundary conditions were created at surfaces next to the blade walls with rotational axis set around the axis $y = 1$.

Pressure outlet boundary condition was set to the same backflow total pressure and total temperature as the pressure inlet with radial pressure distribution enabled.

The first spool up was at 1000 rpm, the time step size was 1e-4 s, 300 time steps were run for a half revolution, then the second spool up was at 2000 rpm, the time step size was 5e-5 s, 300 time steps were run for another

half revolution. Then it was run at the full speed of 2500 rpm with time step size 5e-5 s with 960 time steps for 2 full revolution to spool up the compressor completely. The simulation was then run at 2500 rpm for 480 times steps for the final revolution which was to be analyzed.

The following stage read the area-averaged outlet total pressure, static pressure and total temperature as boundary conditions to be imported. This process repeated for all stages after stage 1.

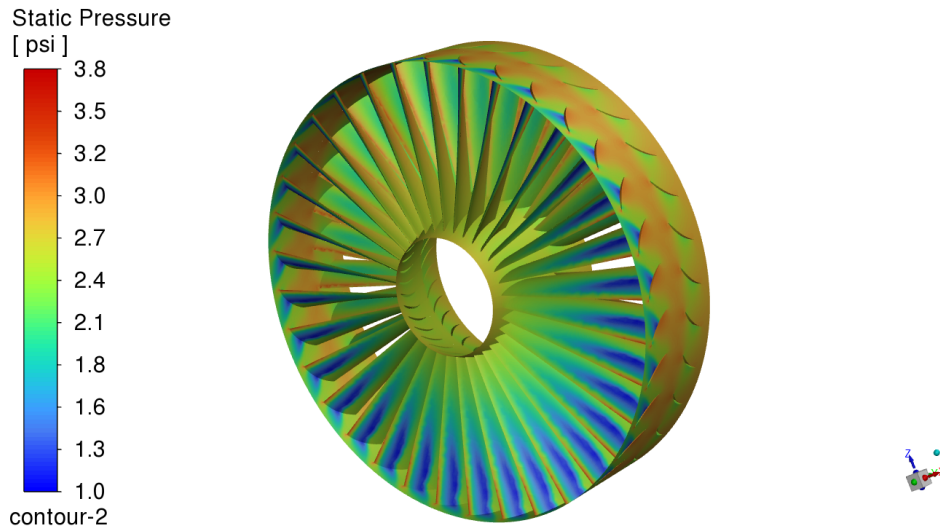


Figure 10: Pressure contour of stage 1 simulation at 40,000 ft above sea level.

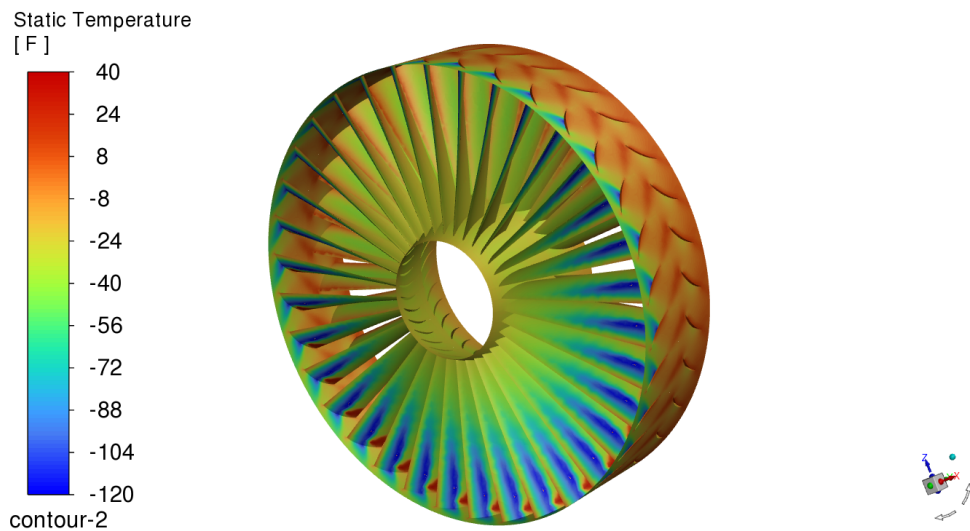


Figure 11: Temperature contour of stage 1 simulation at 40,000 ft above sea level.

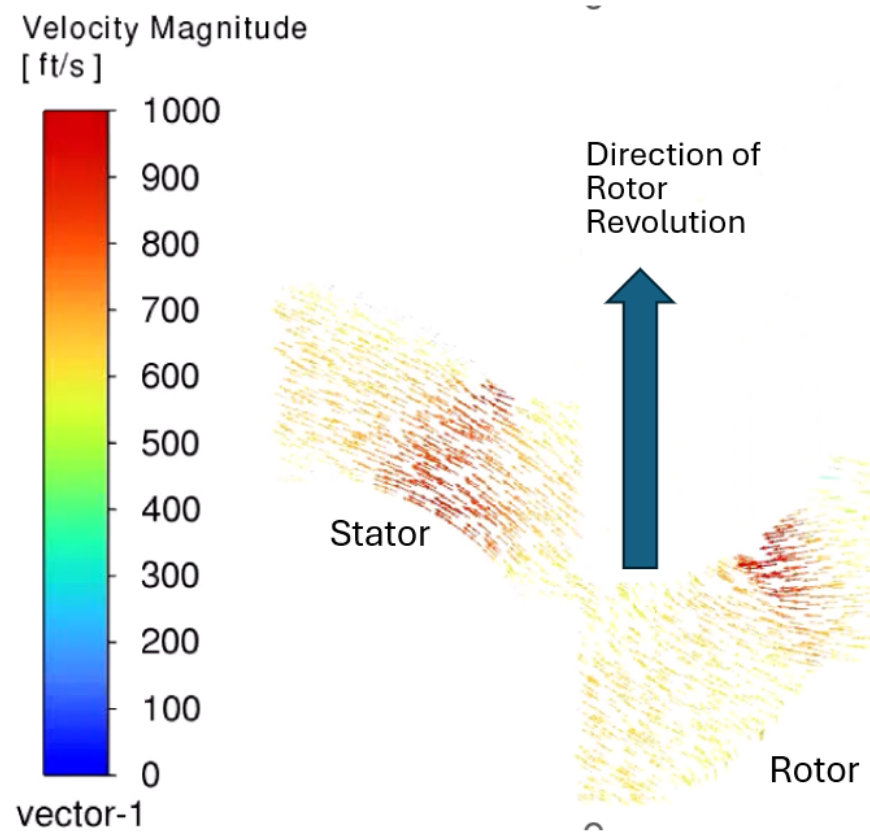


Figure 12: Velocity streamline plot of stage 1 simulation at 40,000 ft above sea level.

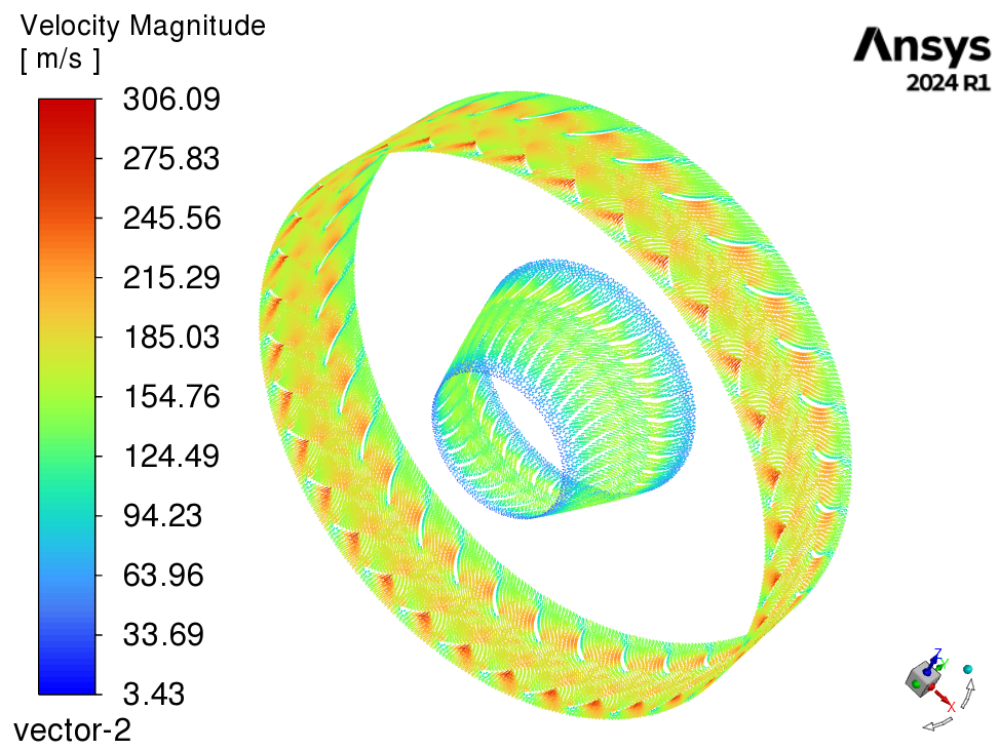


Figure 13: Velocity vector plot of stage 1 simulation at 40,000 ft above sea level.

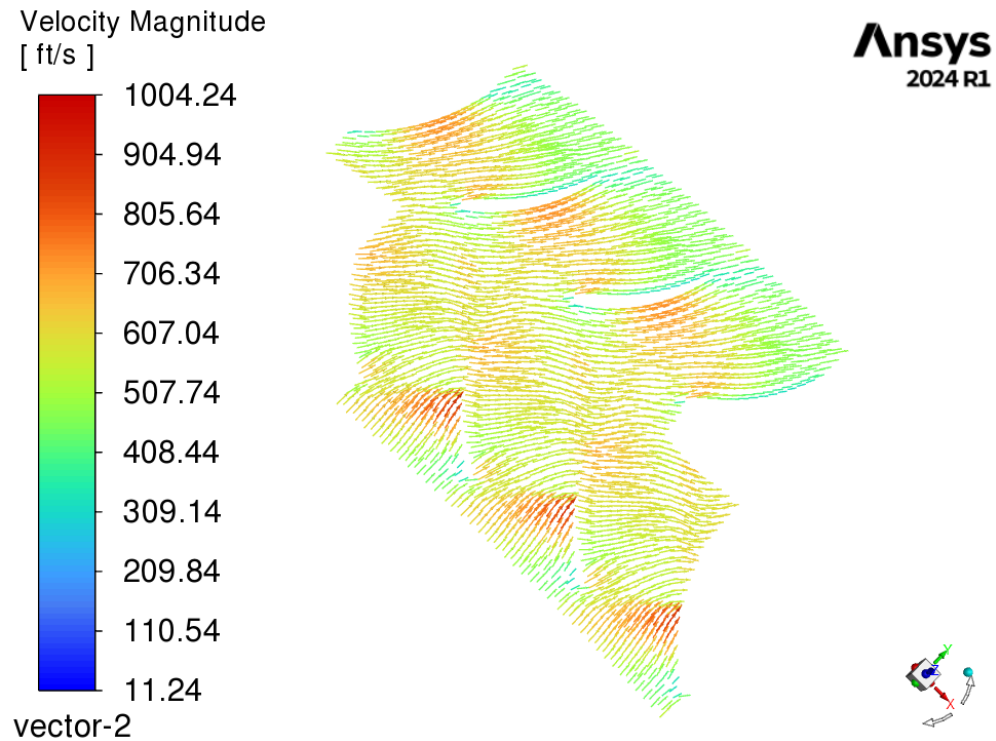


Figure 14: Alternative view of velocity vector plot of stage 1 simulation at 40,000 ft above sea level.

The following plots in Figures 15, 16, 17, 18, display the achieved convergence of the stage 1 simulation. Further convergence plots are shown in **Appendix A**.

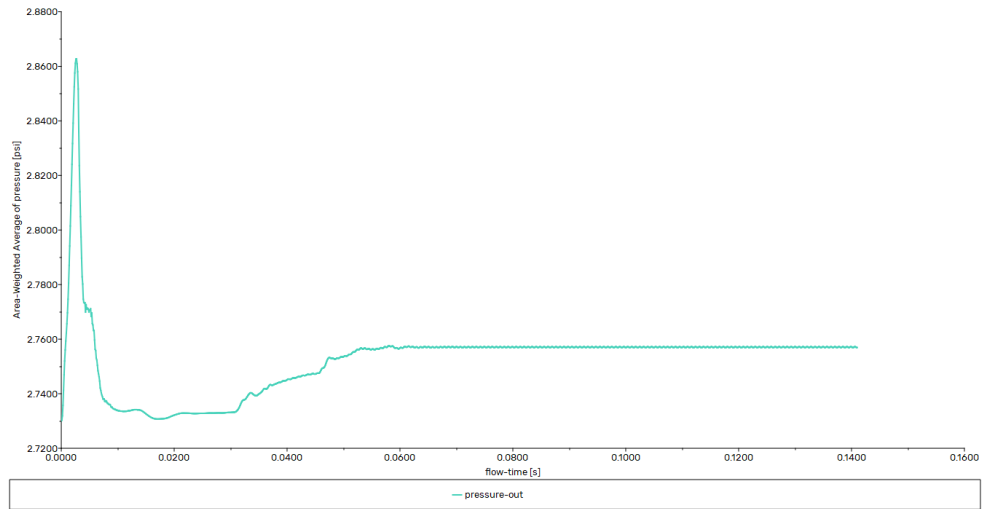


Figure 15: Static pressure convergence plot of stage 1 simulation.

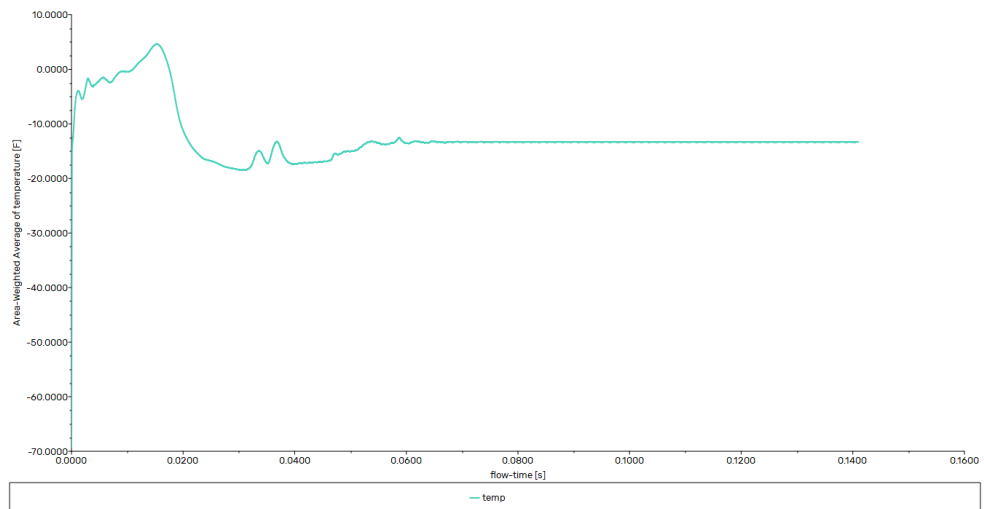


Figure 16: Temperature convergence plot of stage 1 simulation.

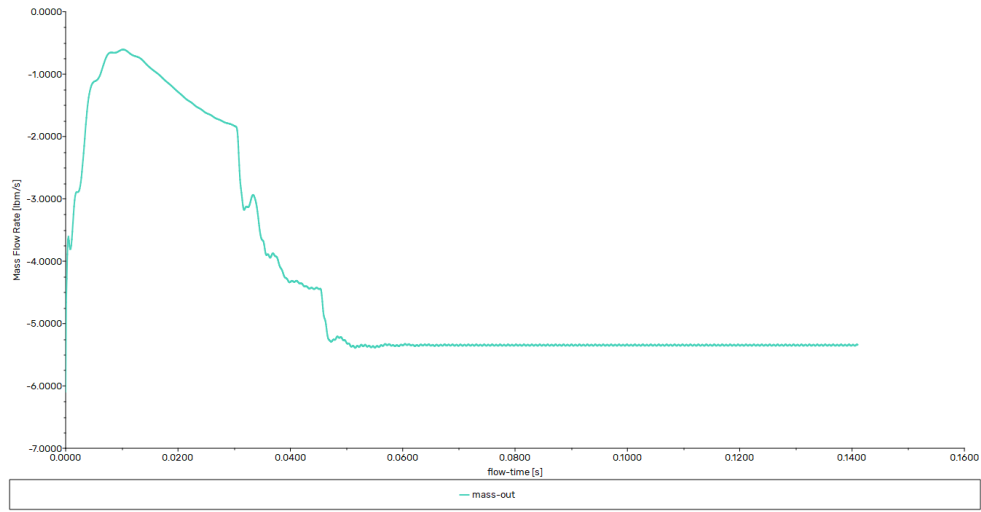


Figure 17: Mass flow rate convergence plot of stage 1 simulation.

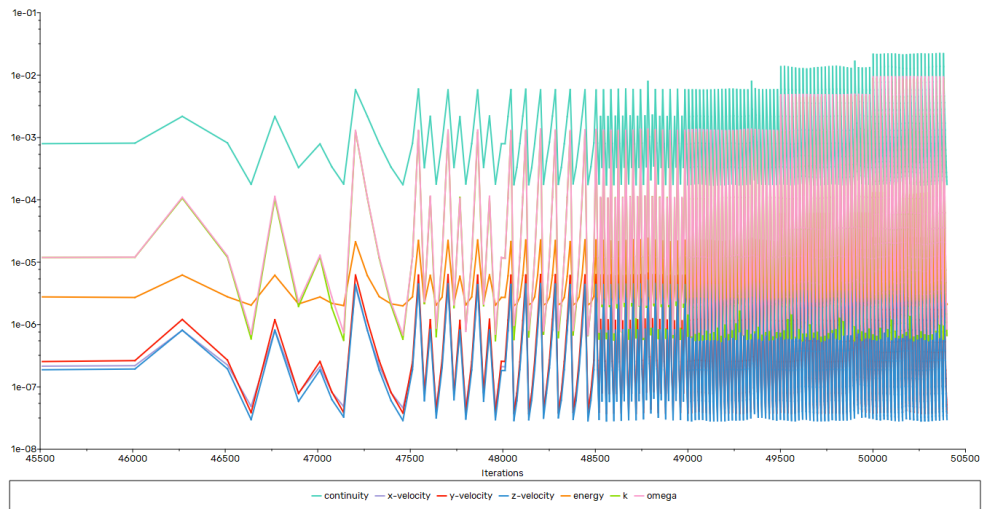


Figure 18: Scaled residual plot of stage 1 simulation.

The next series of figures show the pressure and temperature contour plots for the simulations of stages 2-4.

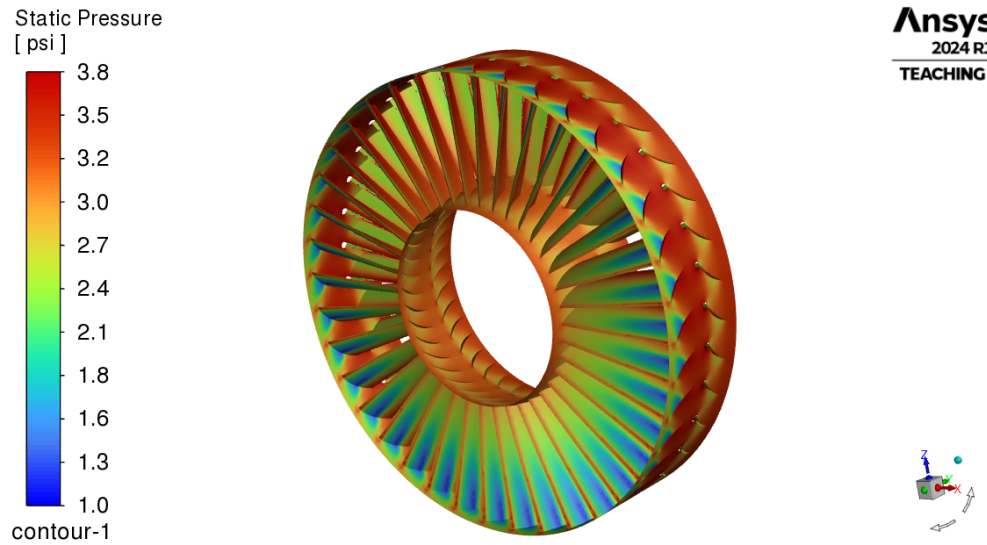


Figure 19: Pressure contour of stage 2 simulation at 40,000 ft above sea level.

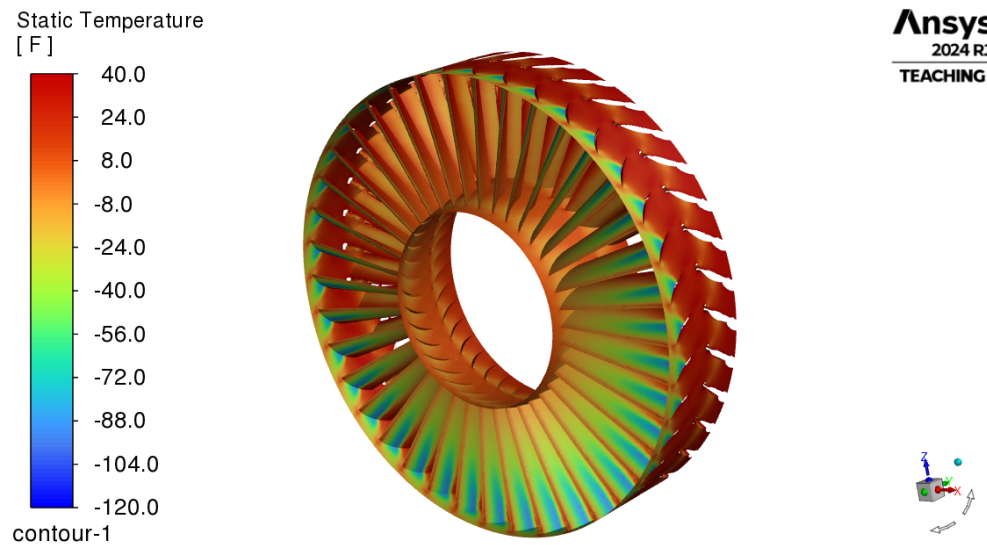


Figure 20: Temperature contour of stage 2 simulation at 40,000 ft above sea level.



Figure 21: Pressure contour of stage 3 simulation at 40,000 ft above sea level.

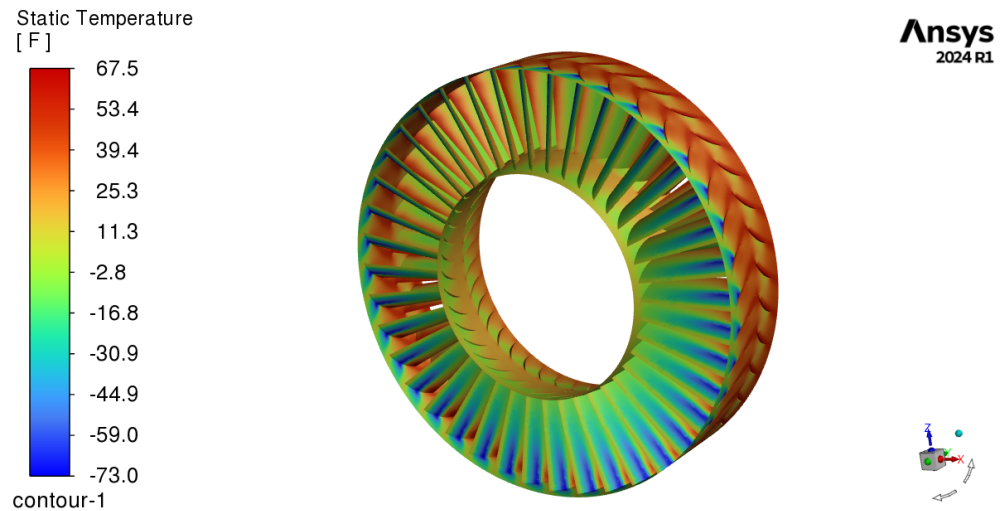


Figure 22: Temperature contour of stage 3 simulation at 40,000 ft above sea level.

At ground level STP, the simulation process was repeated with STP initial conditions for stages 1 and 2.

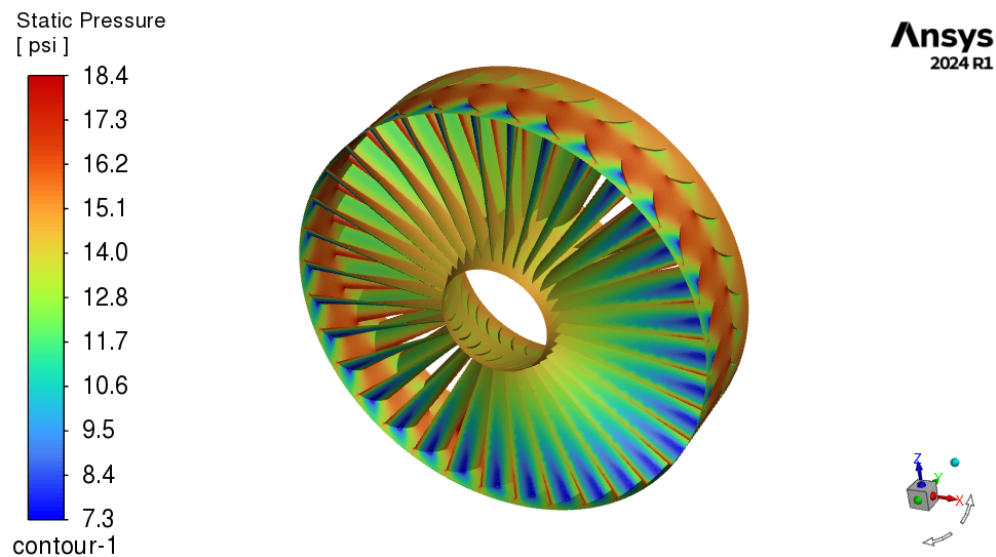


Figure 23: Pressure contour of stage 1 simulation at STP.

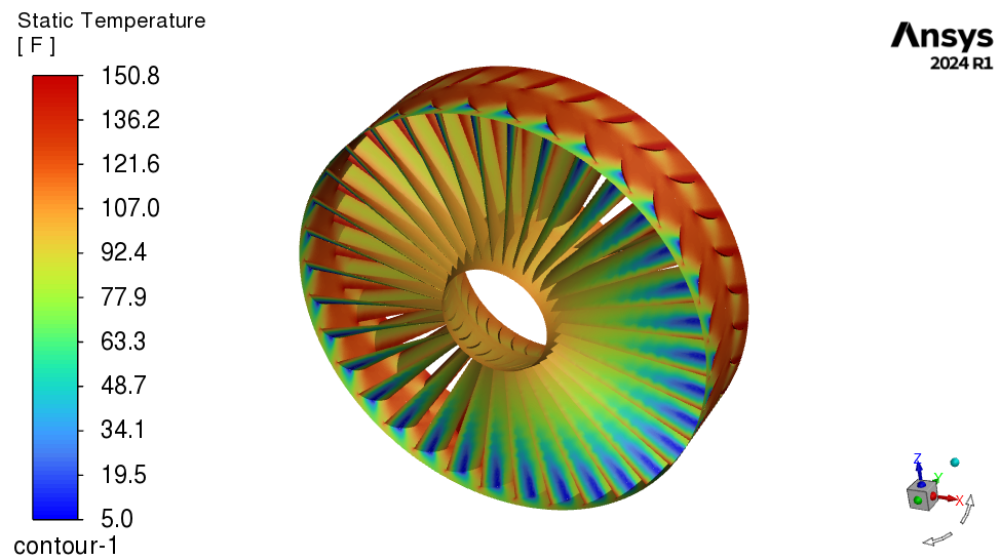


Figure 24: Temperature contour of stage 1 simulation at STP.

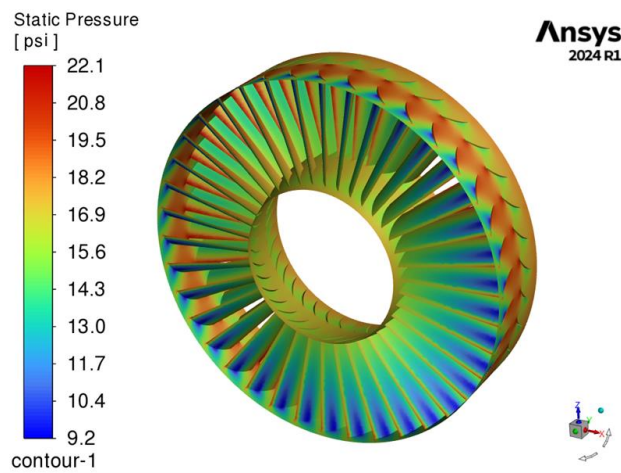


Figure 25: Pressure contour of stage 2 simulation at STP.

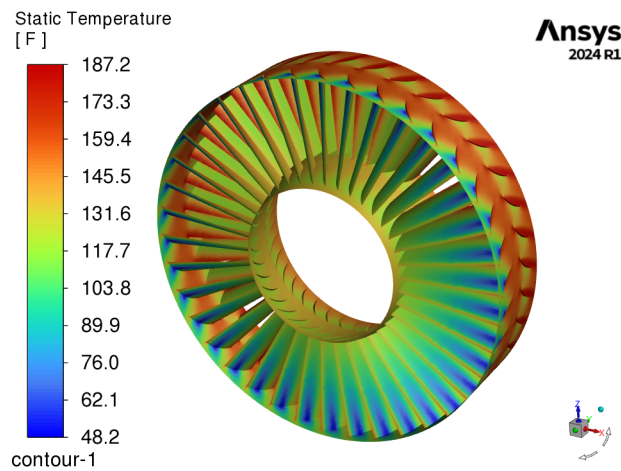


Figure 26: Temperature contour of stage 2 simulation STP.

Model Fitting

The simulation data for the first four stages of the maximum altitude case were used to determine the pre-exponential factor A in the exponential models for pressure and temperature down the compressor. In general, for a thermodynamic quantity Q in an ideal, isentropic compressor, its value at a certain stage is modeled by an exponential relationship.

$$\begin{aligned} Q_{\text{#stages}} &= Q_0 \cdot A^{\#_{\text{stages}}} \\ \implies \ln(Q_{\text{#stages}}) &= \#_{\text{stages}} \cdot \ln(A) + \ln(Q_0) \end{aligned}$$

A linear regression of simulation data can be used to find the particular values of A for pressure $A_P = 1.238$, temperature $A_T = 1.103$, and density $A_\rho =$; In turn we can extrapolate from simulation data.

Results

Results are tabulated for the maximum operating altitude of 40,000 feet in Table 5 and for sea level conditions in Table 6. Comparative simulation and hand calculated values for maximum operating altitude pressures and temperatures per stage are plotted in Figure 27. The efficiency of stage 1 at 40,000 feet is 74%, and at sea level is 71%, further information is tabulated in Figure 28

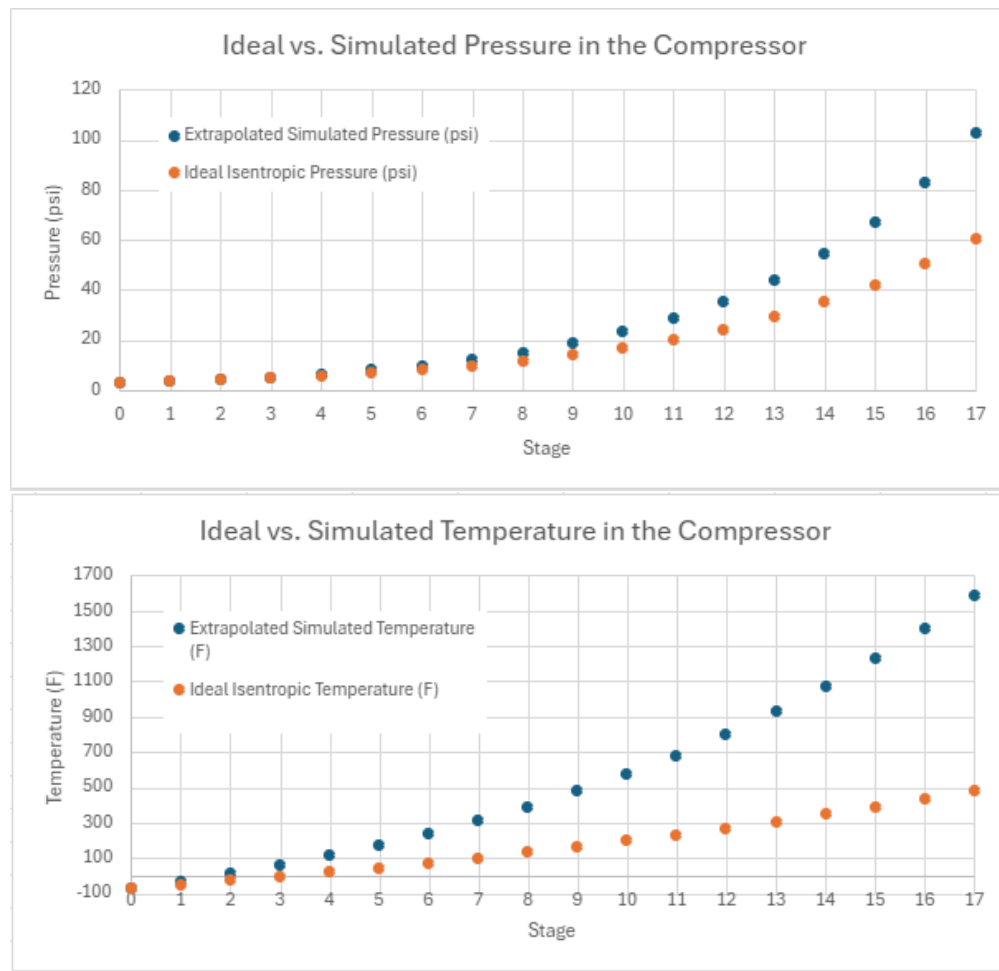


Figure 27: Comparative simulation and hand calculated values for maximum operating altitude pressures and temperatures per stage

40K Stage 1		
RPM	units	2500
Pressure increase	psf	57.6
Mass Flow	lbm/s	5.5
Density	lbm/ft^3	0.0189
volume flow	ft^3/s	291.0053
Power_out	lbf ft/s	16761.90
Omega	rad/s	261.8
Torque	lbf ft	86.157
Power_in	lbf ft rad/s	22555.85
1st Law Eff		74.31%

Sea Level Stage 1		
RPM	units	2500
Pressure increase	psf	345
Mass Flow	lbm/s	24
Density	lbm/ft^3	0.0765
volume flow	ft^3/s	313.7255
Power_out	lbf ft/s	108235.29
Omega	rad/s	261.8
Torque	lbf ft	582
Power_in	lbf ft rad/s	152367.24
1st Law Eff		71.04%

Figure 28: Hand Calculated efficiency calculation for Stage 1 at maximum altitude (top) and sea level (bottom).

Table 5: Results for simulations at maximum operating altitude of 40,000 feet are compared to hand calculations. Quantities with blue infill are extrapolated based on an exponential model fitted with simulation data.

Stage	Sim. Pressure (psi)	Hand Calc. Pressure (psi)	Sim. Total Pressure Ratio	Hand Calc. Total Pressure Ratio	Sim. Temperature (F)	Hand Calc. Temperature (F)
Inlet	2.7	2.7	1.0	1.0	-70	-70
1	3.3	3.3	1.2	1.2	12	-49
2	4.2	3.9	1.5	1.4	21	-27
3	5.2	4.7	1.9	1.7	60	-4
4	6.4	5.7	2.3	2.1	102	20
5	7.9	6.8	2.9	2.5	176	46
6	9.8	8.2	3.6	3.0	241	73
7	12.2	9.8	4.5	3.6	313	101
8	15.1	11.7	5.5	4.3	392	131
9	18.7	14.1	6.8	5.2	479	163
10	23.1	16.9	8.5	6.2	576	196
11	28.6	20.3	10.5	7.4	682	231
12	35.4	24.3	13.0	8.9	799	268
13	43.9	29.2	16.1	10.7	928	307
14	54.3	35.1	19.9	12.8	1071	348
15	67.2	42.1	24.6	15.4	1228	391
16	83.3	50.5	30.5	18.5	1401	436
17	103.1	60.6	37.8	22.2	1592	484

Table 6: Results for simulations at sea level are compared to hand calculations. Quantities with blue infill are extrapolated based on an exponential model fitted with simulation data.

Stage	Sim. Pressure (psi)	Hand Calc. Pressure (psi)	Sim. Total Pressure Ratio	Hand Calc. Total Pressure Ratio	Sim. Temperature (F)	Hand Calc. Temperature (F)
Inlet	14.7	14.7	1.0	1.0	59	59
1	17.8	17.6	1.2	1.2	114	87
2	21.3	21.2	1.2	1.4	148	116
3	23.6	25.4	1.1	1.7	167	147
4	27.9	30.5	1.9	2.1	227	179
5	32.7	36.6	2.2	2.5	277	213
6	38.4	43.9	2.6	3.0	331	249
7	45.0	52.7	3.1	3.6	389	287
8	52.8	63.2	3.6	4.3	450	327
9	62.0	75.8	4.2	5.2	517	369
10	72.7	91.0	4.9	6.2	588	413
11	85.3	109.2	5.8	7.4	664	460
12	100.1	131.0	6.8	8.9	746	509
13	117.4	157.2	8.0	10.7	833	561
14	137.8	188.7	9.4	12.8	928	615
15	161.7	226.4	11.0	15.4	1029	672
16	189.7	271.7	12.9	18.5	1137	733
17	222.6	326.0	15.1	22.2	1253	797

Verification

Thermodynamic Calculations

Atmospheric conditions at 40,000' are summarized in Table 7.

Table 7: Standard conditions and properties of air at an altitude of 40,000 feet [3], [1], [2].

Property	Value	Unit
ρ	0.0189	lbm/ft ³
μ	$9.55 \cdot 10^{-6}$	lbm/ft/s
c_p	0.2405	BTU/lbm/R
c_v	0.1719	BTU/lbm/R
k	0.01149	BTU/hr/lbm/R
T	-69.7	°F
P	2.73	psi

We design for a 1.2:1 stage pressure ratio, which requires at least 17 stages.

$$1.2^{\#_{\text{stages}}} \geq 20$$

$$\#_{\text{stages}} \geq \log_{1.2}(20) = 16.43$$

$$\implies \#_{\text{stages}} \geq 17$$

For thermodynamic calculations, we model the air as an ideal gas. While the inlet condition in Table 7 shows a low-pressure low-temperature system, ideal gas based approximations (tabulated in Table 8) show that the system remains low-pressure but rapidly becomes high-temperature, which is an acceptable condition to

approximate a real gas as ideal.

Table 8: Tabulated inlet and outlet conditions after 17 stages based on ideal, isentropic compressor approximation.

Property	Inlet	Outlet	Units
T	389.97	943.5	R
P	2.73	60.57	psi
ρ	0.0189	0.1733	lbm/ft ³

We can apply the following relations to compute the change in temperature in an isentropic approximation of our compressor. For a constant $\gamma = c_p/c_v = 1.399$ matching the inlet conditions (Table 7), we expect the following behavior across a stage

$$T_2 = T_1 \cdot \left(\frac{P_2}{P_1} \right)^{\frac{\gamma-1}{\gamma}} = 1.05335 T_1$$

$$\rho_2 = \rho_1 \cdot \left(\frac{P_2}{P_1} \right)^{\frac{1}{\gamma}} = 1.13922 \rho_1$$

This means that across the compressor we expect

$$P_{\text{out}} = P_{\text{in}} \cdot 1.2^{\# \text{stages}}$$

$$T_{\text{out}} = T_{\text{in}} \cdot 1.05335^{\# \text{stages}}$$

$$\rho_{\text{out}} = \rho_{\text{in}} \cdot 1.13922^{\# \text{stages}}$$

Vane & Blade Design Calculations

Angles of Attack

The blade cross-section is NACA 9506, the angle of attack is $\alpha_1 = 13^\circ$. Following standard convention, useful angles may be computed following trigonometric formulas.

$$\theta_1 = \arctan\left(\frac{\omega \cdot r_1}{v_{\text{inlet}}}\right) = 48.423^\circ$$

$$\theta_2 = \arctan\left(\frac{\omega \cdot r_2}{v_{\text{inlet}}}\right) = 5.168^\circ$$

$$\alpha_2 = \arctan\left(\frac{v - w_1 \sin(\beta_2)}{w_1 \cos(\beta_2)}\right)$$

$$\beta_2 = \arctan\left(\frac{v + v_0 \sin(\alpha_1)}{v_0 \cos(\alpha_2)}\right)$$

$$w_1 = \frac{v_1 \cos(\alpha_1)}{\cos(\beta_1)}$$

$$\alpha_{2H} = \arctan\left(\frac{v - w_1 \sin(\beta_2)}{w_1 \cos(\beta_2)}\right)$$

Speeds

We design for v_{inlet} as 80% of Mach 1 and operating RPM ω to be 2500 rpm.

$$v_{\text{inlet}} = 0.8M_1 = 774.17 \text{ ft/s} = 9289.98 \text{ in/s}$$

The velocity of an object rotating at a distance r from its attachment point with angular velocity ω is

$$s = 2\pi r\omega$$

for which our speeds of interest are at the blade tip where $r = \frac{d_0}{2}$ and the hub attachment where $r = \frac{d_i}{2}$.

Reynolds Numbers

Generally the Reynolds number is defined in terms of density ρ , velocity u , a characteristic length L , and a viscosity μ .

$$Re = \rho u \frac{L}{\mu}$$

The main variable between systems is the definition of characteristic length.

For the flow around our airfoils, the characteristic length is the chord length, 6".

The characteristic length for the flow in the axial direction is the hydraulic diameter, defined in terms of cross-sectional area A and wetted perimeter P of the region of interest, in our case the annulus of fluid

between the outer shell and the hub.

$$L = D_H = \frac{4A}{P} = \frac{4 \cdot \pi(d_o^2 - d_i^2)}{\pi d_o + \pi d_i} = \frac{4 \cdot \pi \cdot (d_o + d_i) \cdot (d_o - d_i)}{\pi \cdot (d_o + d_i)} = d_o - d_i$$

$$s_{r_1} = \omega \cdot r_1 = 10471.98 \text{ in/s}$$

$$s_{r_2} = \omega \cdot r_2 = 35081.12 \text{ in/s}$$

Which means the air speed (including inlet velocity) is

$$s_{r_1, \text{ total}} = \sqrt{s_{r_1}^2 + v_{\text{inlet}}^2} = 13998.79 \text{ in/s} = 1.2055 \text{ M}$$

$$s_{r_2, \text{ total}} = \sqrt{s_{r_2}^2 + v_{\text{inlet}}^2} = 36290.34 \text{ in/s} = 3.125115 \text{ M}$$

Efficiency Calculations

The volumetric flow rate in the axial direction is product of the axial velocity v and annular area A . The power used to compress this volumetric flow rate across each stage is $E_{\text{actual}} = \dot{V}\Delta P$.

For an ideal situation, the change in enthalpy $\Delta H = c_p\Delta T$, and the ideal power usage is

$$E_{\text{ideal}} = \Delta H \cdot \dot{V} \cdot \rho$$

The efficiency of a stage is the ratio of the ideal power to the actual power

$$\begin{aligned} \eta &= \frac{E_{\text{ideal}}}{E_{\text{actual}}} \\ &= \frac{\Delta H \cdot \dot{V} \cdot \rho}{\dot{V}\Delta P} \\ &= \frac{c_p\Delta T\rho}{\Delta P} \\ &= \frac{c_p(T_2 - T_1)\rho}{\Delta P} \end{aligned}$$

Conclusion

The axial compressor had a composite compression ratio of 37.8:1, which met the requirement of 20:1. The average isentropic efficiency per stage was 82.4%. The total power consumed by the compressor was 1087 hp at 40000 ft, and 4902 hp at sea level.

Design Time

The design, simulations, and report took about 400 hours to complete.

References

- [1] *Air - Specific Heat vs. Pressure at Constant Temperature* — engineeringtoolbox.com. https://www.engineeringtoolbox.com/air-specific-heat-various-pressure-d_1535.html. [Accessed 30-04-2025]. 2001.
- [2] *Air Properties - Thermal Conductivity vs. Temperature and Pressure Charts and Calculator* — engineeringtoolbox.com. https://www.engineeringtoolbox.com/air-properties-viscosity-conductivity-heat-capacity-d_1509.html. [Accessed 30-04-2025]. 2001.
- [3] *U.S. Standard Atmosphere: Temperature, Pressure, and Air Properties vs. Altitude* — engineeringtoolbox.com. https://www.engineeringtoolbox.com/standard-atmosphere-d_604.html. [Accessed 30-04-2025]. 2001.

Appendix A: Maximum Altitude Simulation Results by Submodel

Scaled residual and convergence plots for each simulated stage at maximum altitude. *s1*

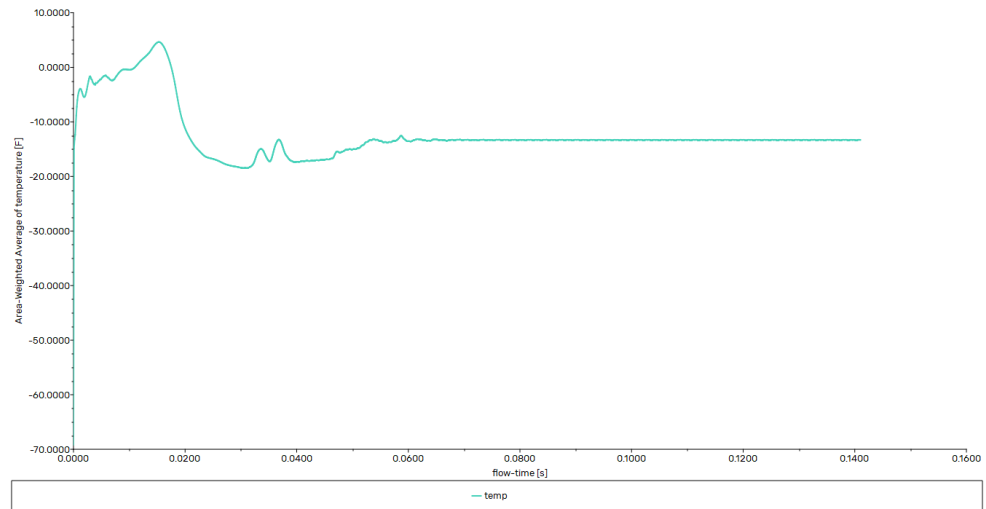


Figure 29: Temperature convergence plot at stage 1.

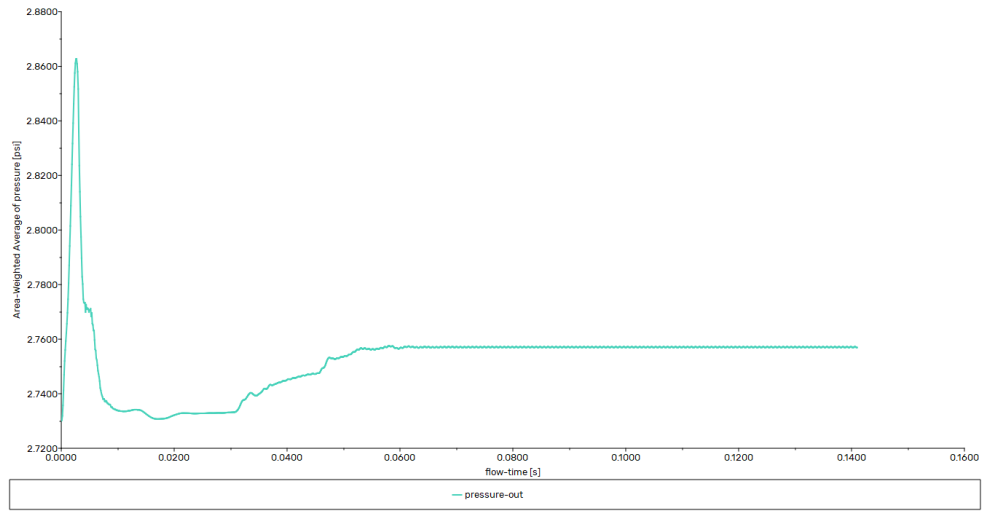


Figure 30: Pressure convergence plot at stage 1.

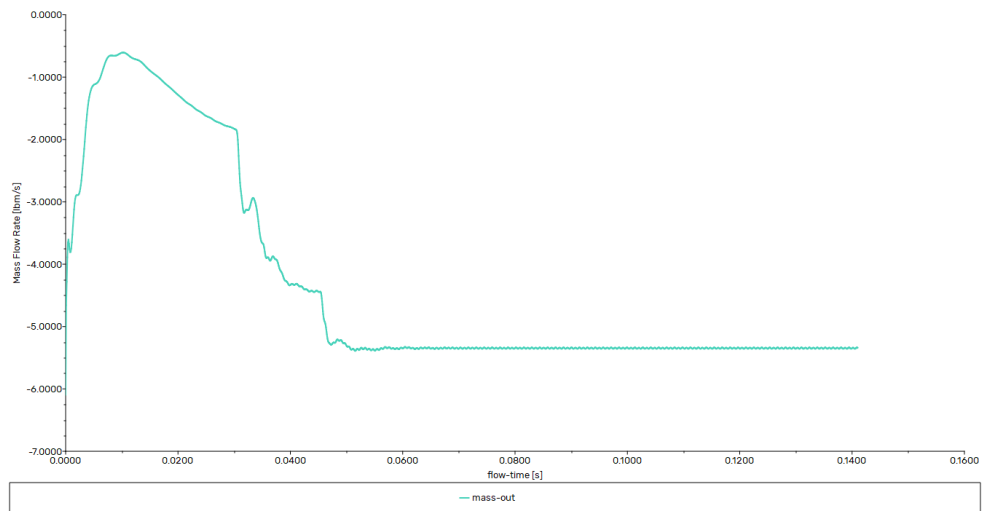


Figure 31: Mass flow rate convergence plot at stage 1.

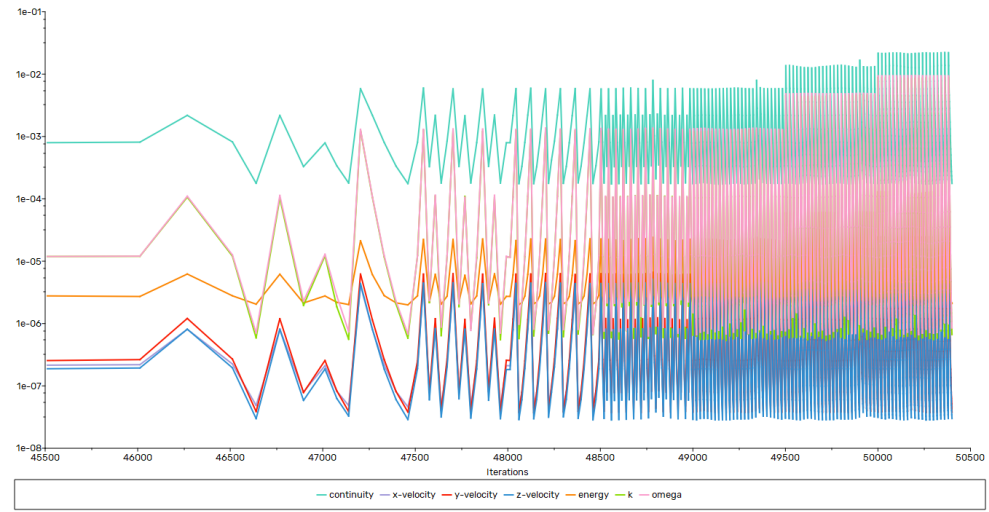


Figure 32: Scaled residual plot at stage 1.

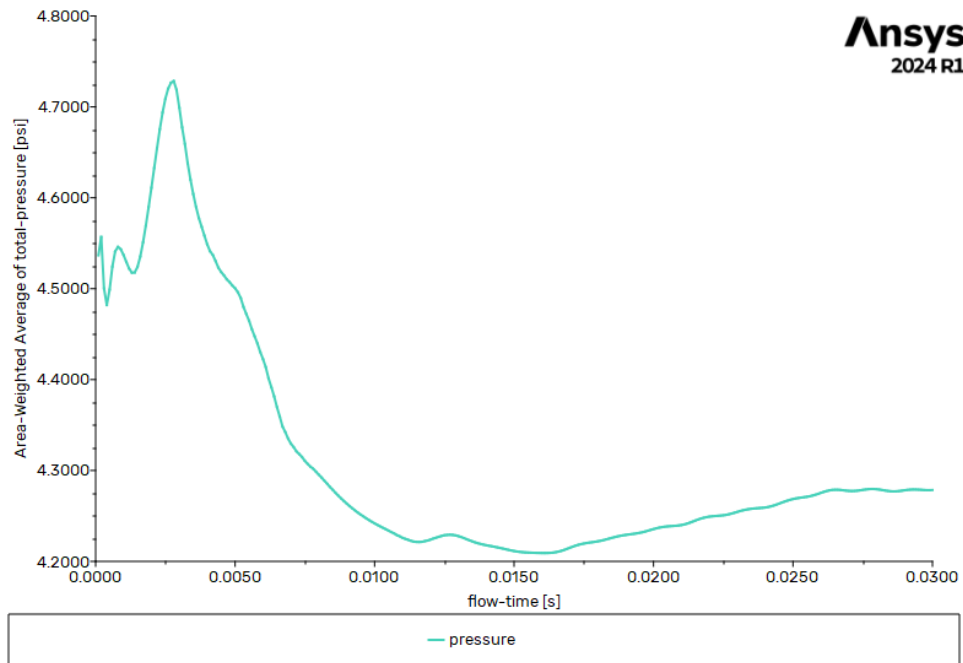


Figure 33: Pressure convergence plot at stage 2.

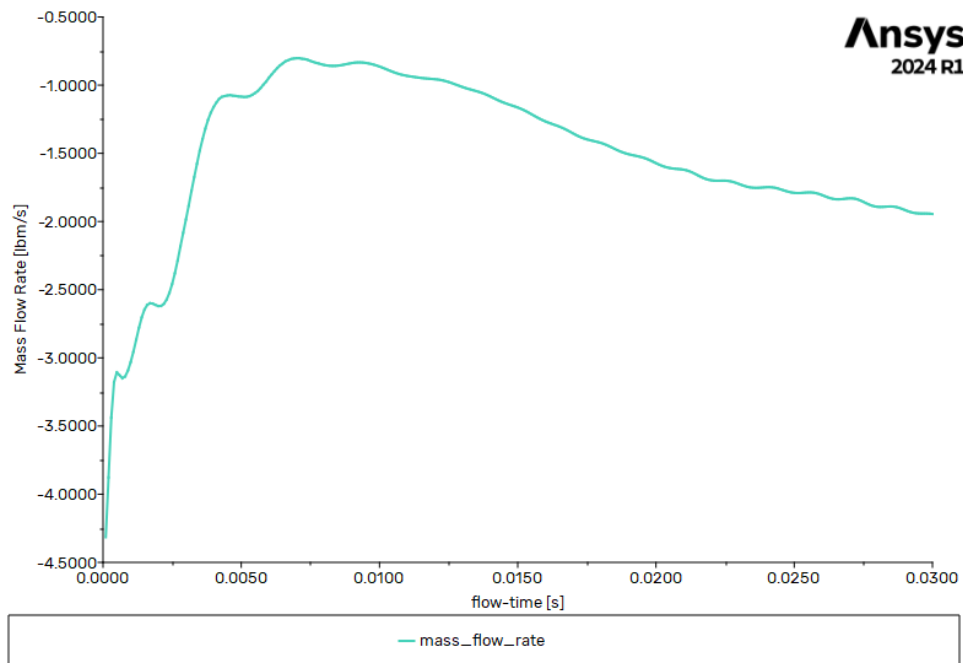


Figure 34: Mass flow rate convergence plot at stage 2.

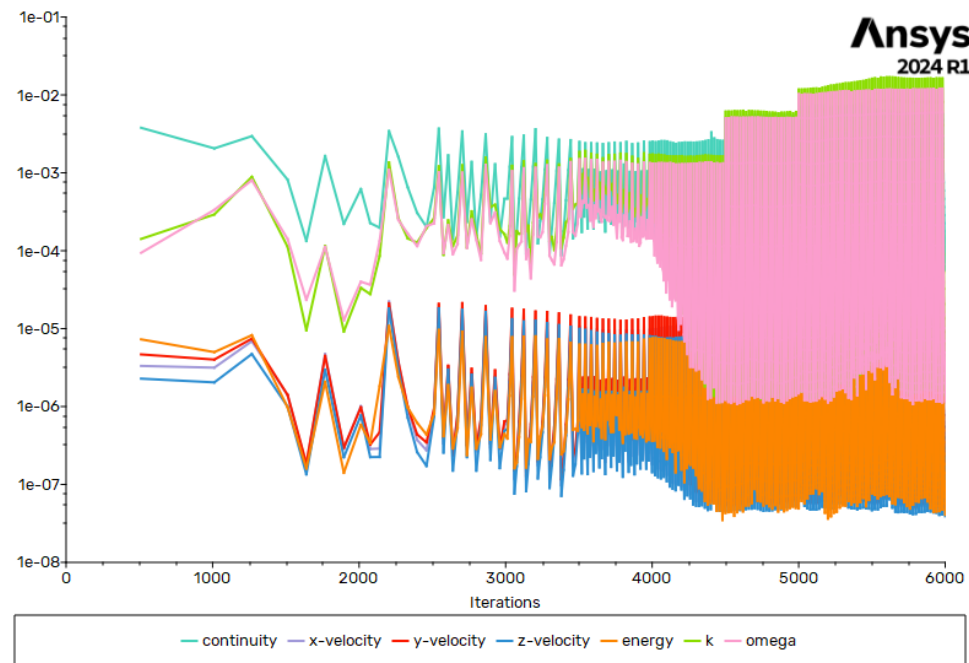


Figure 35: Scaled residual plot at stage 2.

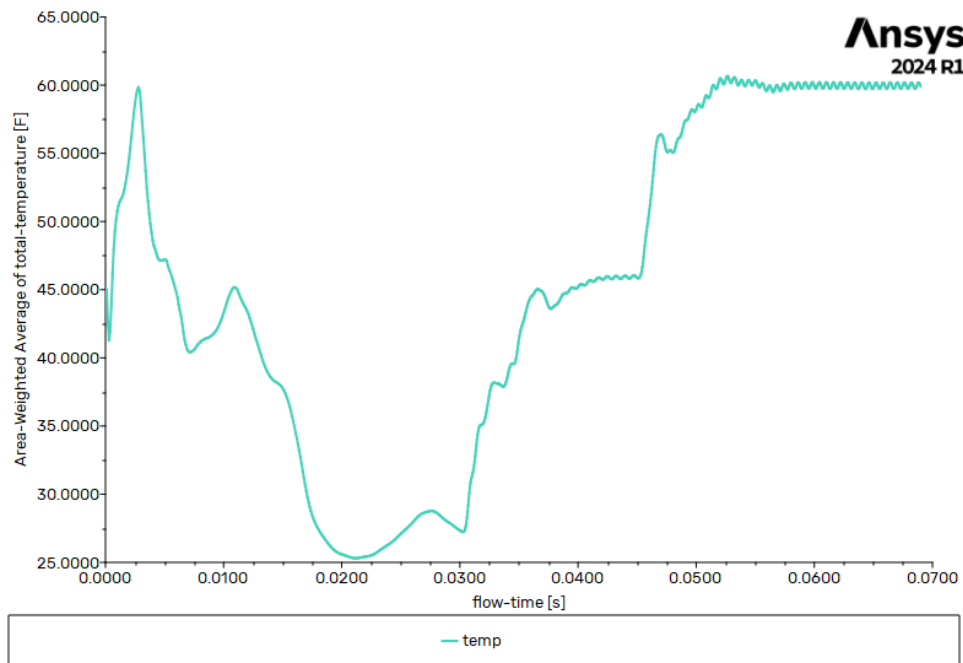


Figure 36: Temperature convergence plot at stage 3.

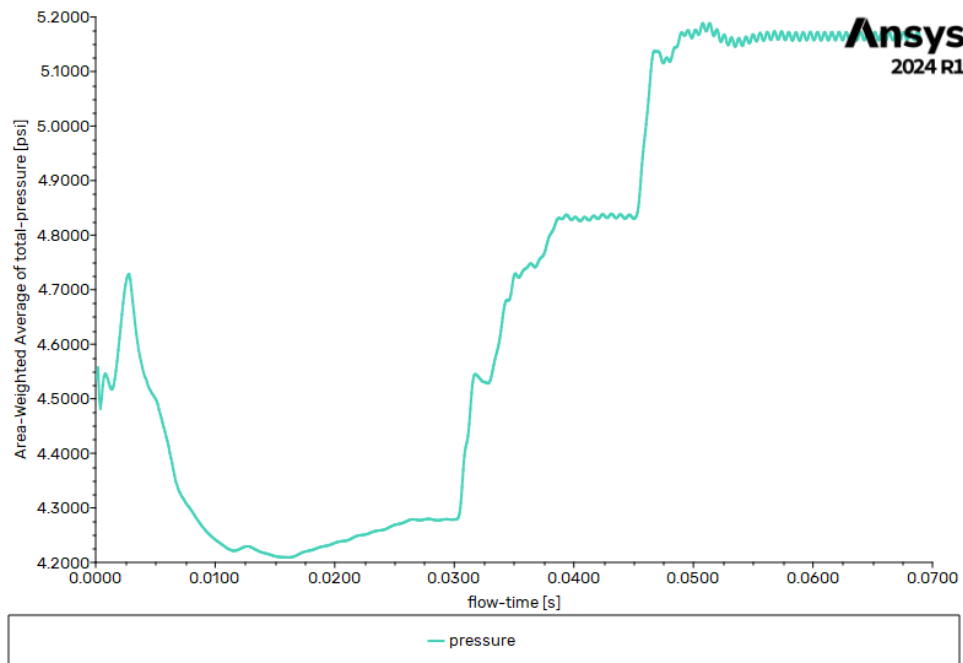


Figure 37: Pressure convergence plot at stage 3.

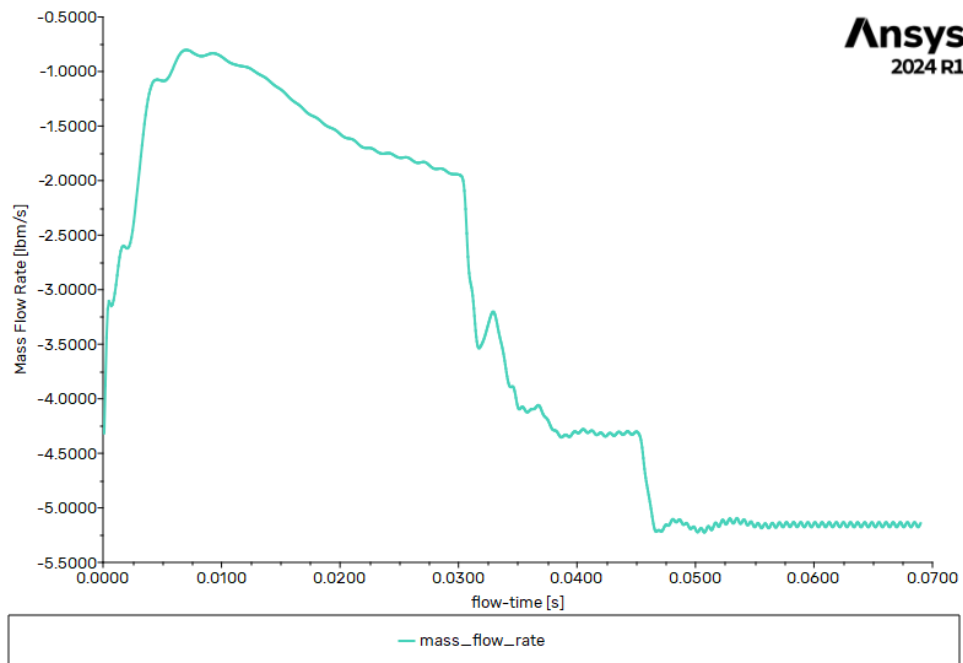


Figure 38: Mass flow rate convergence plot at stage 3.

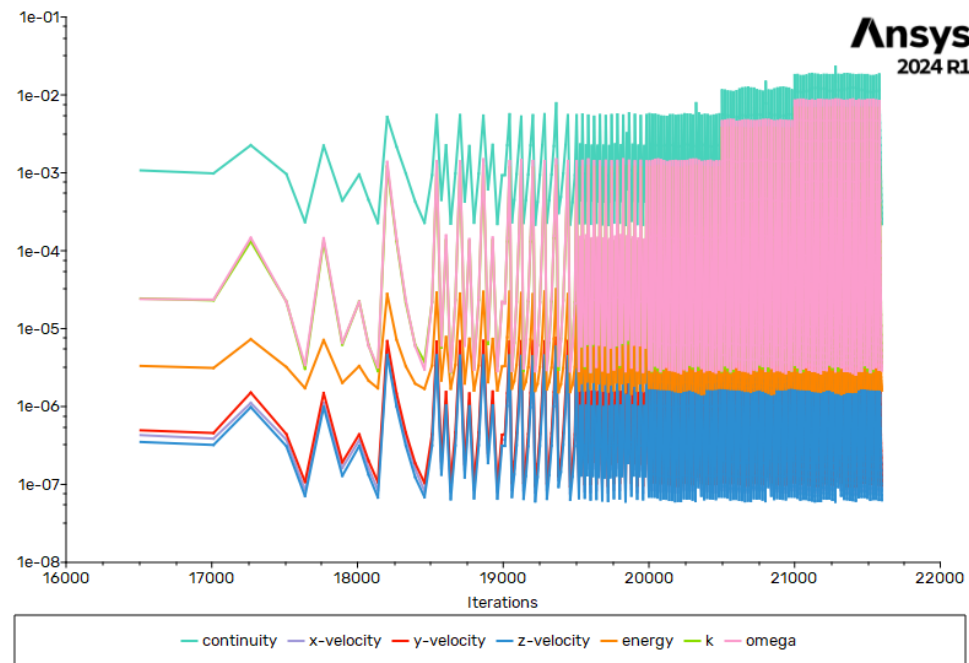


Figure 39: Scaled residual plot at stage 3.

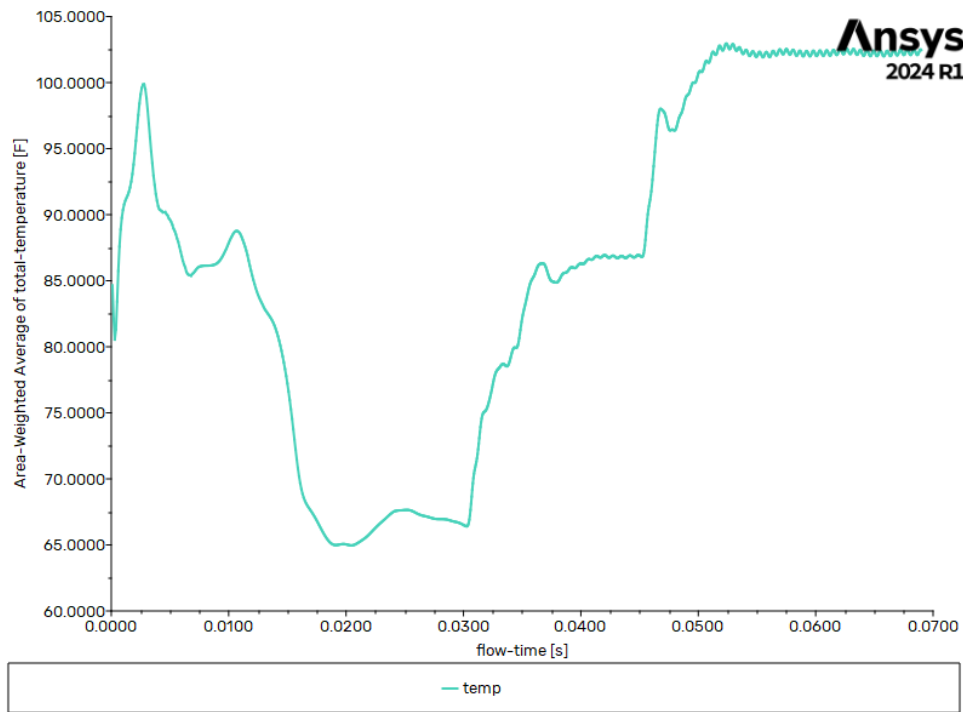


Figure 40: Temperature convergence plot at stage 4.

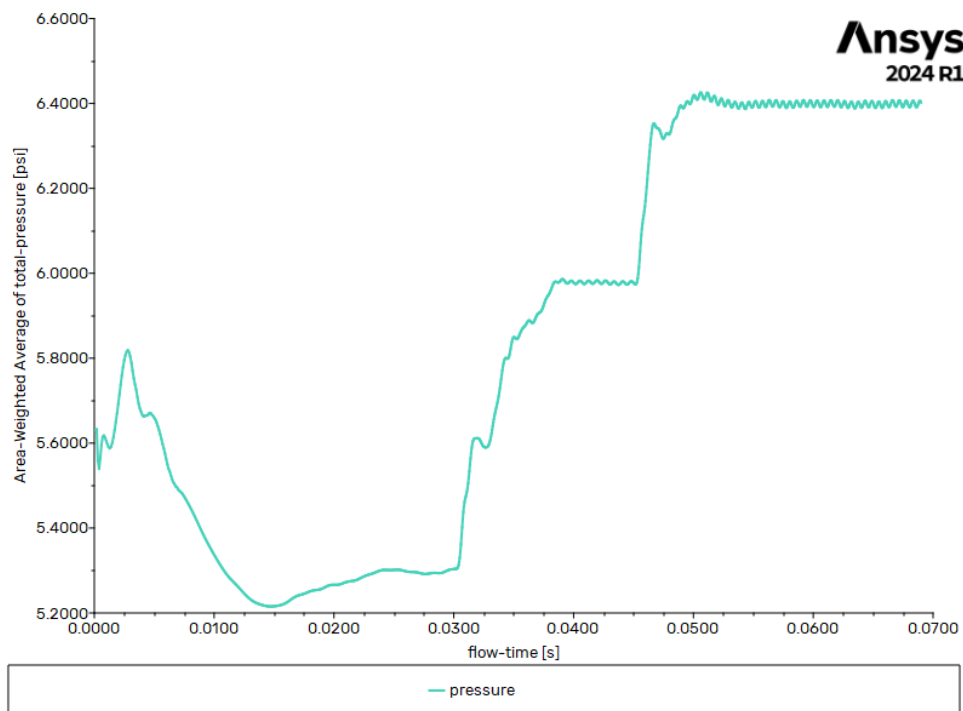


Figure 41: Pressure convergence plot at stage 4.

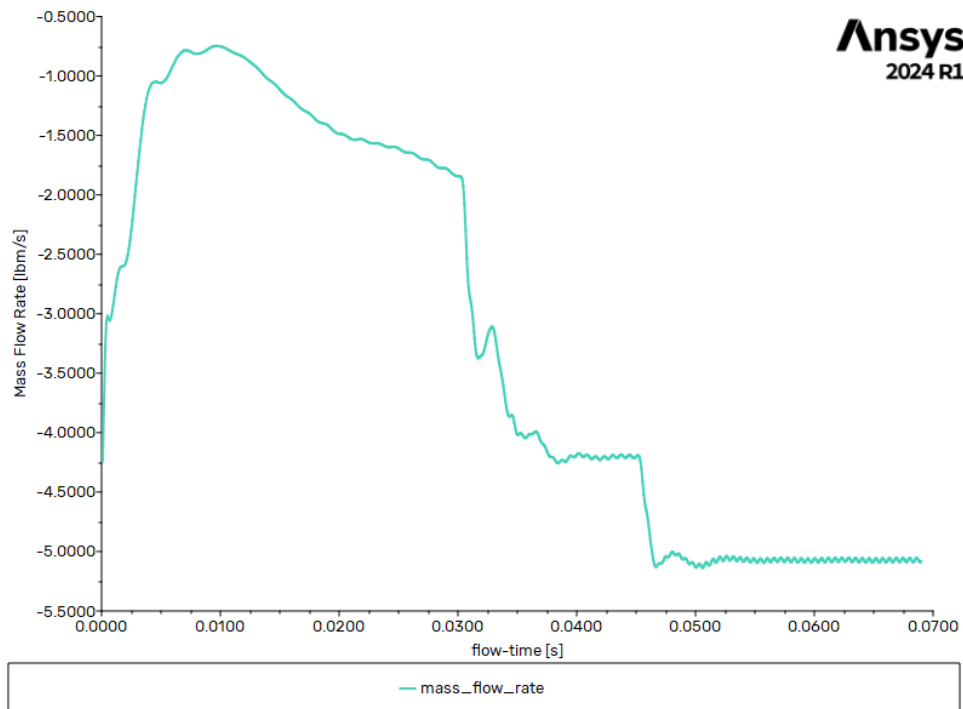


Figure 42: Mass flow rate convergence plot at stage 4.

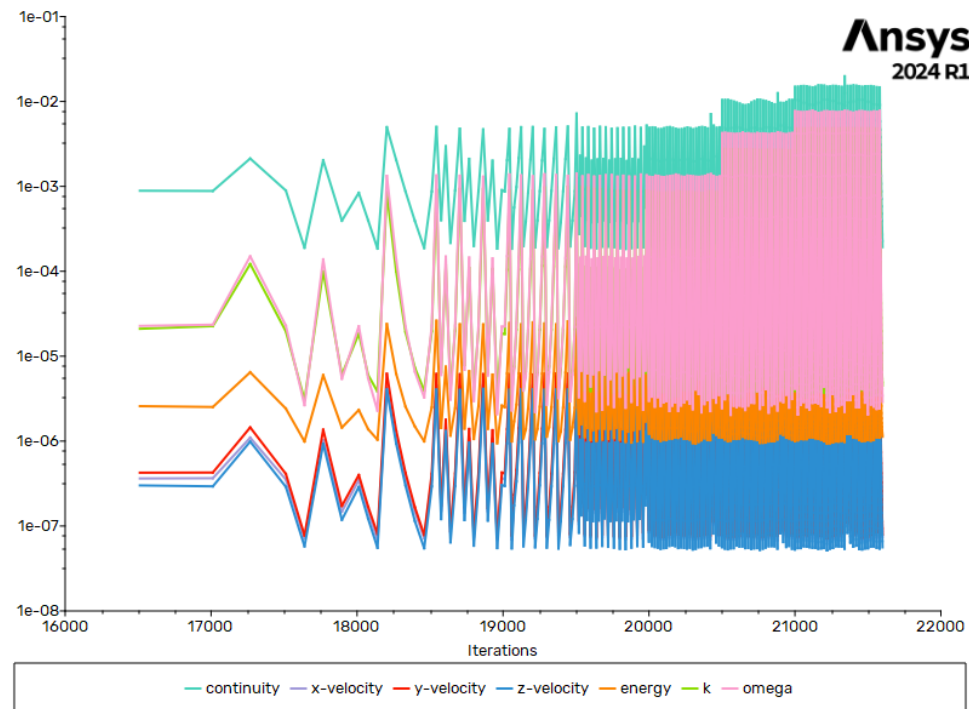


Figure 43: Scaled residual plot at stage 4.

Appendix B: Sea Level Simulation

Results by Submodel

Scaled residual and convergence plots for each simulated stage at ground level.

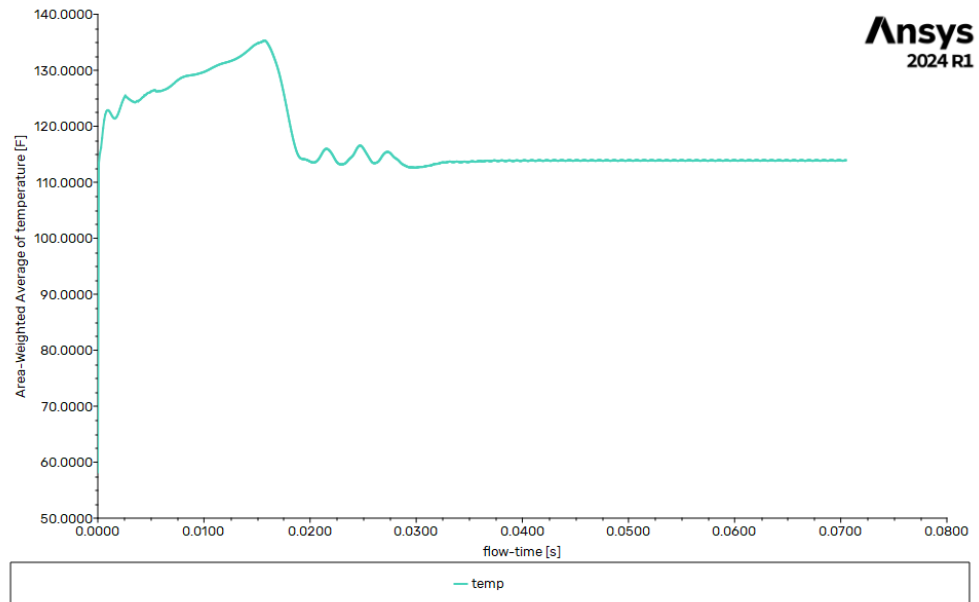


Figure 44: Temperature convergence plot at stage 1 at ground.

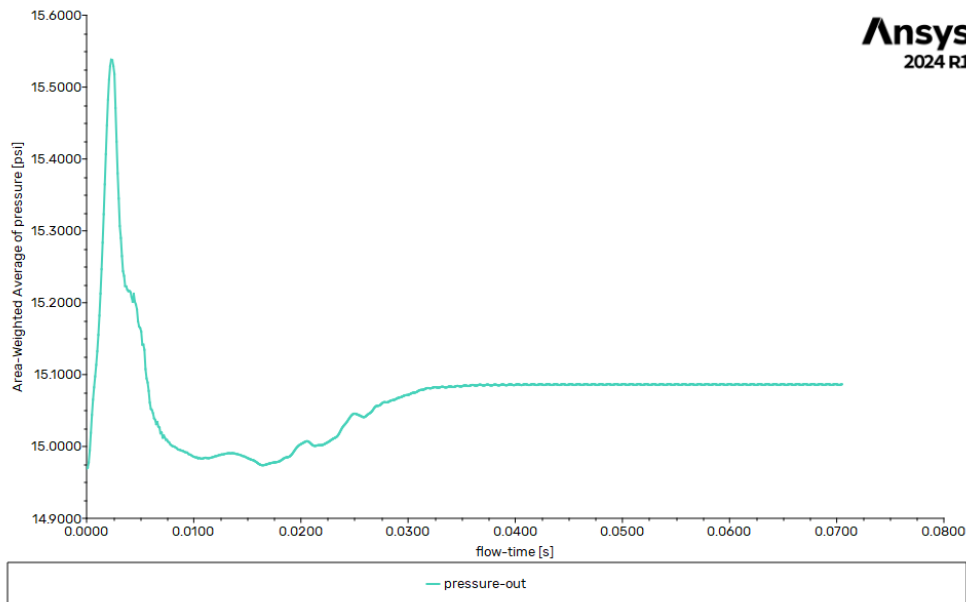


Figure 45: Pressure convergence plot at stage 1 at ground.

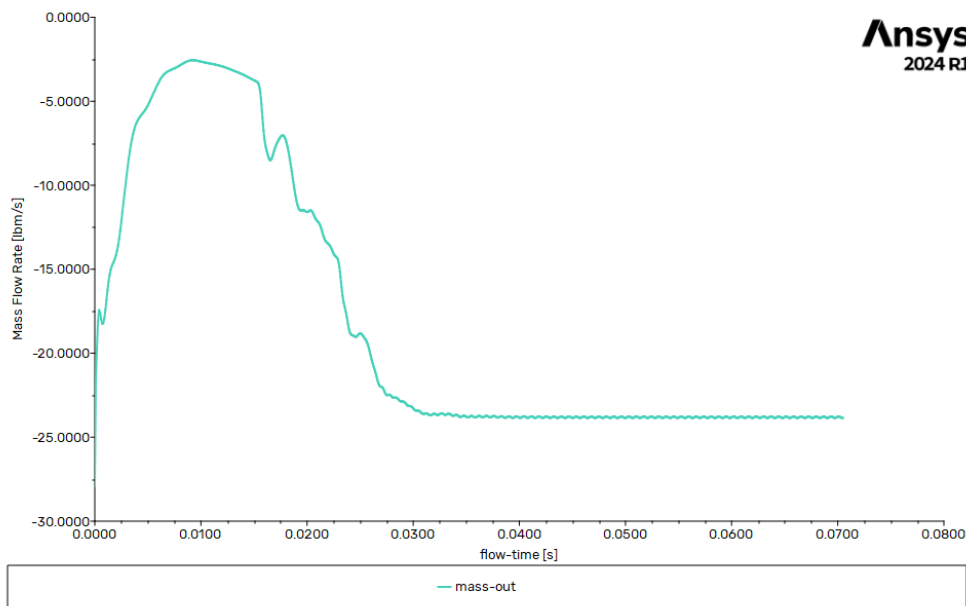


Figure 46: Mass flow rate plot at stage 1 at ground.

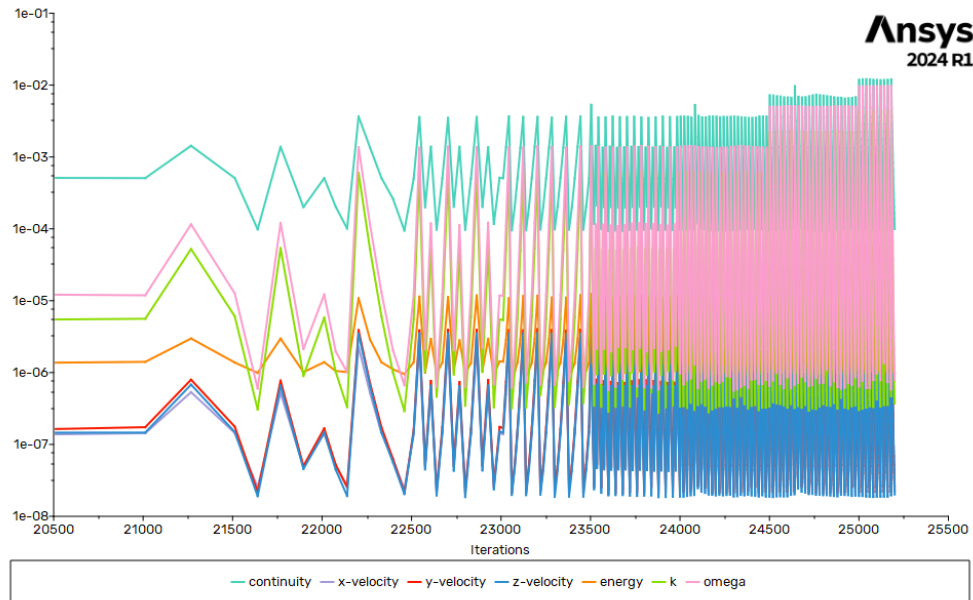


Figure 47: Scaled residual plot at stage 1 at ground.

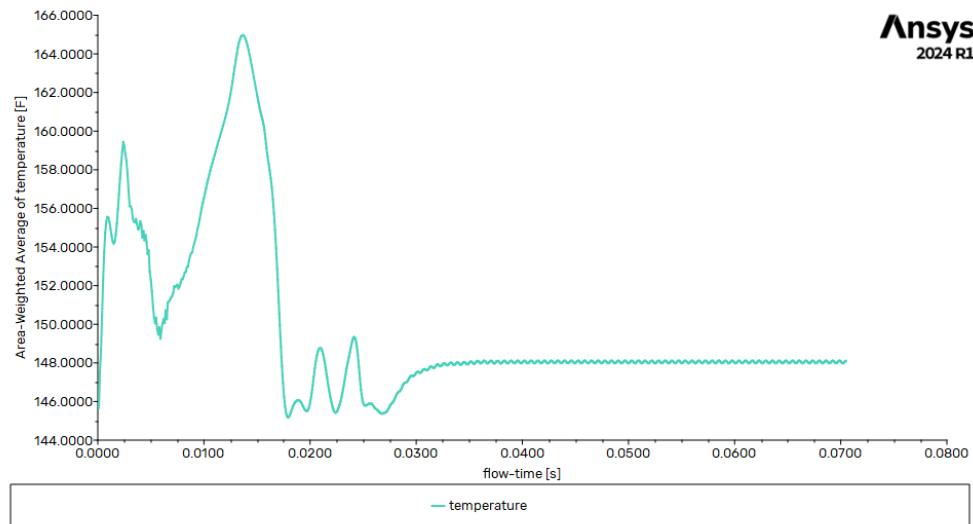


Figure 48: Temperature convergence plot at stage 2 at ground.

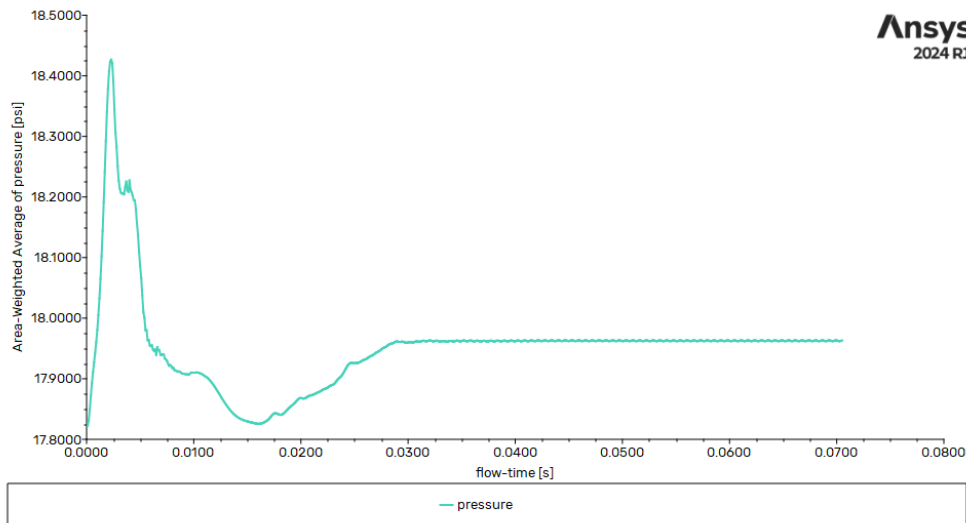


Figure 49: Pressure convergence plot at stage 2 at ground.

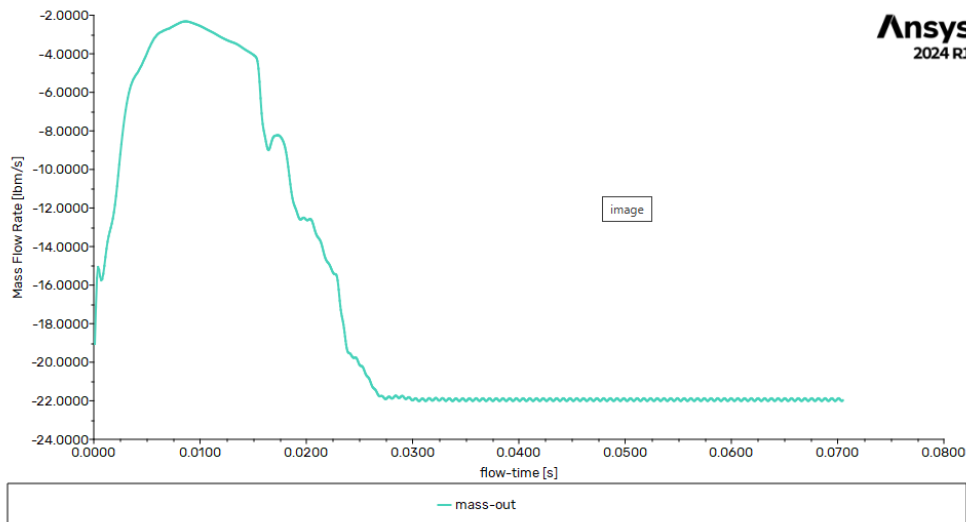


Figure 50: Mass flow rate plot at stage 2 at ground.

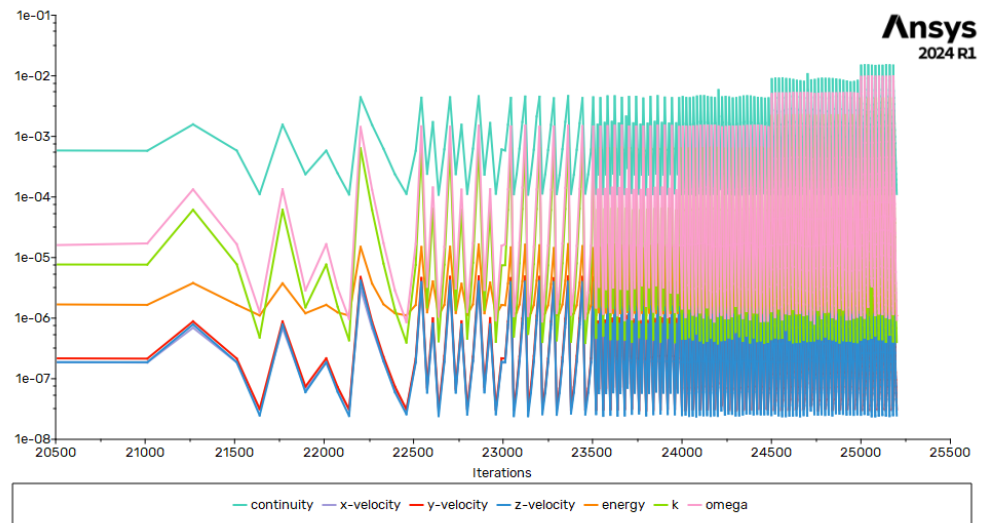


Figure 51: Scaled residual plot at stage 2 at ground.